



**HAL**  
open science

# Climatology of Nighttime Medium-Scale Traveling Ionospheric Disturbances at Mid and Low Latitudes Observed by the DEMETER Satellite in the Topside Ionosphere During the Period 2005–2010

Chien-Thang Nguyen, Jean-Jacques Berthelier, Monique Petitdidier, Christine Amory-Mazaudier, Minh Le Huy

## ► To cite this version:

Chien-Thang Nguyen, Jean-Jacques Berthelier, Monique Petitdidier, Christine Amory-Mazaudier, Minh Le Huy. Climatology of Nighttime Medium-Scale Traveling Ionospheric Disturbances at Mid and Low Latitudes Observed by the DEMETER Satellite in the Topside Ionosphere During the Period 2005–2010. *Journal of Geophysical Research Space Physics*, 2022, 127 (10), pp.e2022JA030517. 10.1029/2022JA030517 . insu-03831293

**HAL Id: insu-03831293**

**<https://insu.hal.science/insu-03831293>**

Submitted on 11 Apr 2023

**HAL** is a multi-disciplinary open access archive for the deposit and dissemination of scientific research documents, whether they are published or not. The documents may come from teaching and research institutions in France or abroad, or from public or private research centers.

L'archive ouverte pluridisciplinaire **HAL**, est destinée au dépôt et à la diffusion de documents scientifiques de niveau recherche, publiés ou non, émanant des établissements d'enseignement et de recherche français ou étrangers, des laboratoires publics ou privés.

Copyright

# JGR Space Physics

## RESEARCH ARTICLE

10.1029/2022JA030517

### Key Points:

- Medium-scale traveling ionospheric disturbances (MSTID) maps provide statistical evidence of the major role of Es in local summer MSTID development and their inter-hemispheric conjugacy
- Unexpected inter-hemispheric asymmetry in response to solar activity put in evidence from South/North MSTID occurrence ratio at solstices
- Results obtained from a study of worldwide MSTID seasonal variations from 2005 to 2010 using O<sup>+</sup> ion data from the Detection of Electro-Magnetic Emissions Transmitted from Earthquake Regions satellite

### Correspondence to:

C. T. Nguyen,  
thang0405@gmail.com

### Citation:

Nguyen, C. T., Berthelier, J.-J., Petitdidier, M., Amory-Mazaudier, C., & Le Huy, M. (2022). Climatology of nighttime medium-scale traveling ionospheric disturbances at mid and low latitudes observed by the DEMETER satellite in the topside ionosphere during the period 2005–2010. *Journal of Geophysical Research: Space Physics*, 127, e2022JA030517. <https://doi.org/10.1029/2022JA030517>



Received 6 APR 2022

Accepted 5 OCT 2022

### Author Contributions:

**Investigation:** C. T. Nguyen, J.-J. Berthelier, M. Petitdidier, C. Amory-Mazaudier

## Climatology of Nighttime Medium-Scale Traveling Ionospheric Disturbances at Mid and Low Latitudes Observed by the DEMETER Satellite in the Topside Ionosphere During the Period 2005–2010

C. T. Nguyen<sup>1,2</sup> , J.-J. Berthelier<sup>2</sup> , M. Petitdidier<sup>2</sup>, C. Amory-Mazaudier<sup>3</sup> , and M. Le Huy<sup>1</sup>

<sup>1</sup>Institute of Geophysics, Vietnam Academy of Science and Technology, Hanoi, Vietnam, <sup>2</sup>Sorbonne Université, LATMOS/IPSL/CNRS, UPMC, Paris, France, <sup>3</sup>Sorbonne Université, LPP, CNRS-UPMC-Ecole Polytechnique, UPMC, Paris, France

**Abstract** Thermal ion measurements from the French Detection of Electro-Magnetic Emissions Transmitted from Earthquake Regions micro-satellite have been used to study the climatology of nighttime Medium-scale traveling ionospheric disturbances (MSTIDs) in the topside ionosphere at 650 km altitude during the 6 years of the satellite operation, from 2005 to 2010. This period encompasses the declining phase of solar cycle 23, the deep solar minimum of 2008–2009 and the early rise of solar cycle 24. MSTIDs were detected from the quasi-periodic variations of the density of the dominant ionospheric O<sup>+</sup> ions. Mostly present between ~15° and ~40° invariant latitudes with a small number of events in equatorial regions, the MSTIDs exhibit, on the average, larger occurrence rates in the Southern hemisphere with a peak in the Eastern Pacific-South America longitude sector. The dependence of MSTID activity on solar activity appears more complex than the previously reported simple anti-correlation. In addition to year-to-year variations, our study has, in particular, put in evidence a noticeable hemispheric asymmetry in the seasonal variations during the deep solar minimum of 2008–2009. These statistical observations provide a remarkable observational support to the key role of sporadic Es layers and the conjugate mapping of the associated electric fields. Yet, improved theoretical and numerical models, taking into account the actual inter-hemispheric differences of the seasonal and solar activity variations of thermospheric and ionospheric processes, are needed for a better understanding of the highly complex MSTID phenomena.

**Plain Language Summary** Night-time Medium scale traveling ionospheric disturbances (MSTIDs) are quasi-periodic spatial structures of the plasma density that develop at nighttime at mid to low latitudes from the bottom of the F-region to the topside ionosphere. The long series of thermal ion measurements performed on-board the Detection of Electro-Magnetic Emissions Transmitted from Earthquake Regions satellite from 2005 to 2010 have been used to study their climatology. Several new features of the MSTID activity and occurrence areas and their seasonal and yearly variations have been revealed, in particular during the deep solar minimum of 2008–2009. Contributing to a more accurate and detailed knowledge of the MSTID climatology, they provide a remarkable observational support to the key role of sporadic Es layers and the conjugate mapping of the associated electric fields. They also show that upgraded theoretical and numerical models, representative of the seasonal and solar activity dependence of thermospheric and ionospheric processes, are needed for a better understanding of MSTID phenomena.

## 1. Introduction

Medium scale traveling ionospheric disturbances (MSTIDs), characterized by quasi-periodic spatial variations of the plasma density extending from the lower F-region to the topside ionosphere, are one of the major phenomena taking place in the nighttime ionosphere at mid and low latitudes. Detected long ago from the induced disturbances on HF radio-wave propagation (Du Castel & Faynot, 1964), they have been intensively studied with the advent of modern ground-based and satellite observational techniques. Following a study by Behnke (1979) with the Arecibo IS radar, HF-Doppler receivers, radars and satellite beacons (Jacobson et al., 1995; Ogawa et al., 1994; Shibata & Okuzawa, 1983) provided initial observations.

Over the last two decades, the complexity and importance of MSTID phenomena in the field of ionospheric plasma physics and its coupling with the neutral upper atmosphere aroused a large number of studies which

benefited from the continuous improvement of observational techniques. All-sky imagers at 630 nm, that produce high resolution 2D maps of OI emissions from the dissociative recombination of molecular oxygen  $O_2^+$  at an altitude of  $\sim 250$  km directly representative of the plasma structures, have been extensively used in different longitude sectors: in Japan (Saito et al., 2001; Shiokawa, Ihara, Otsuka, & Ogawa, 2003), Central Pacific area (Duly et al., 2013), Brazil (Amorim et al., 2011) and Central America (Martinis et al., 2010). TEC measurements by dense networks of GPS receivers, free from meteorological and local time limitations, probe the ionosphere close to the maximum of the F-region at 300–350 km altitude. Thanks to elaborate processing algorithms (e.g., Beach et al., 1997), nearly continuously 2D maps of the ionosphere have been obtained over Japan (Saito, Fukao, & Miyazaki, 1998), USA (Kotake et al., 2007; Tsugawa et al., 2007) and China (Ding et al., 2011) and simultaneously over 6 distant sites in Japan, Europe, Eastern and Western USA, South America and Australia (Kotake et al., 2006). Optical and TEC observations have been combined by Saito et al. (2001) and Huang et al. (2016) to provide a more thorough description of the MSTID structures. Ionospheric HF radars, in particular the Super Darn network, brought several new observations (Frissell et al., 2014; Grocott et al., 2013; Ishida et al., 2008; Moffat-Griffin et al., 2011) and a novel observational technique, based on the analysis of phase fluctuations of VHF emissions from radio-sources recorded by the VLA radio-telescope, was reported by Helmboldt and Intema (2012).

Worldwide coverage has been allowed by low Earth Orbit (LEO) satellite observations which, due to their large orbital velocity, provide nearly instantaneous snapshot of the plasma density structures over several spatial wavelengths along the orbit track (e.g., Park et al., 2010; Shiokawa, Ihara, Otsuka, Ogawa, et al., 2003). Events characterized by intensified fluctuations of electric (MEF) or magnetic fields (MMF) were identified as the signatures of MSTIDs by Saito et al. (1995), Saito, Iyemori, et al. (1998) and by Park et al. (2009), Park et al. (2016) from the CHAMP and SWARM satellite data.

As an average picture, in the Northern hemisphere MSTID fronts are elongated along a NW-SE direction and propagate toward SW with a low velocity of  $\sim 50$ – $120$  m/s. Their spatial wavelengths range from  $\sim 100$  to  $\sim 500$  km with local plasma density variations of  $\sim 15\%$ – $30\%$  relative to background in the topside ionosphere. Similar characteristics are observed in the Southern hemisphere with a symmetrical geometrical configuration with respect to the equator so that the Southern MSTID fronts are, on the average, elongated along the SW-NE direction and propagate toward NW. Inter-hemispheric studies have shown that MSTIDs often occur simultaneously over magnetically conjugate regions (Otsuka et al., 2004; Shiokawa et al., 2005) as also evidenced from satellite observations (Burke et al., 2016).

In a pioneering work Perkins (1973) showed that quasi-periodic disturbances may develop in the unstable nighttime mid-latitude F-region with an orientation close to the MSTID front orientation. However, the computed growth rate is far too small to account for the amplitude of the measured plasma density variations. Theoretical efforts to identify the processes that may yield large enough growth rates were initially performed by Kelley and Fukao (1991) and later completed by Garcia et al. (2000), Kelley et al. (2000) and Kelley and Makela (2001). These authors put in evidence the role of polarization electric fields in the development and motion of plasma undulations.

Subsequent theoretical and modeling studies by Tsunoda and Cosgrove (2001), Cosgrove and Tsunoda (2004), Tsunoda et al. (2004), Tsunoda (2006), Yokoyama et al. (2009), Yokoyama and Hysell (2010), Yokoyama (2013) have shown that the enhanced ionospheric conductivities and electric fields associated with sporadic Es layers and mapped along magnetic field lines connecting the E and F regions, may act efficiently to increase the growth rates and generate large amplitude MSTIDs in the F-layer. In a similar way, Yokoyama (2014) have shown that electrostatic coupling along the Earth's magnetic field allows electric fields present at one end of a magnetic field line to map to the conjugate ionosphere and offer favorable conditions for MSTIDs to develop in the conjugate area.

Atmospheric gravity waves (AGWs) are considered as a potential seeding mechanism: in the E-region, they induce wind shears that may give rise to sporadic Es layers and, in the F-region, they generate plasma irregularities that help the coupled E-F regions instabilities to develop. Most AGW arise from tropospheric or stratospheric sources (jet stream, cold fronts, thunderstorms, orographic waves, ocean waves etc...) and propagate upward in the thermosphere or deposit their energy in the mesosphere to generate secondary waves that further propagate at higher altitudes (Vadas and Becker, 2018, 2019; Vadas et al., 2018). Due to the major importance of propagation and the overall complexity of atmospheric and ionospheric processes, fully developed ionospheric disturbances

cannot, in general, be directly compared with local mesospheric AGW (e.g., Huang et al., 2016). Yet, an interesting statistical correlation have been recently obtained by Tsuchiya et al. (2020) in a comparative study of AGW and MSTID wave number spectra and their seasonal and solar cycle variations. In addition, by separating dark band MSTIDs from periodic MSTIDs at low latitudes, Figueiredo et al. (2018) were led to distinguish two classes of events relying on different physical mechanisms: they concluded that events classified as periodic MSTIDs should arise from the F-region plasma disturbances induced by upward propagating AGW.

In this paper we report a detailed statistical study of the climatology of nighttime mid and low latitude MSTIDs observed in the topside ionosphere along the 650 km altitude, nearly sun synchronous orbit of DEMETER at a local time of  $22.00 \pm 0.5$  hr. In the following, the term MSTID will refer to nighttime MSTIDs. This study was performed using mainly thermal ion measurements from the Plasma Analyzer Instrument (IAP) during the 6-year period of the satellite operation from 2005 to 2010. This period covers the fall of solar cycle 23 in 2005–2007 with declining solar and magnetic activities, the deep solar minimum in 2008 and 2009 and the rise of solar and magnetic activities in 2010 early in the new solar cycle 24. After a brief overview of IAP and its modes of operation, we describe the method used to detect MSTID events and the data processing to determine their main characteristics. We then present the main outcomes of our study such as the geographical distribution of the occurrence areas, the influence of solar and magnetic activities, the seasonal and inter-annual variations of the events and their inter-hemispheric conjugacy. In a last section we discuss these statistical results in the light of current models of MSTID generation and development.

## 2. The DEMETER Satellite and Instrumentation

DEMETER, the first satellite in the Myriad program of the French Center National d'Etudes Spatiales (CNES), was primarily devoted to the search and identification of possible pre-earthquake disturbances in the ionosphere (Parrot, 2006). Launched from Baïkonour (Russia) on 29 June 2004 on a circular quasi-sun synchronous polar orbit with  $98^\circ$  inclination and at an initial altitude of 710 km, lowered to 650 km early in 2006, DEMETER was 3-axis stabilized and Earth-pointing with a full set of instruments to measure the thermal ionospheric electron and ion populations, the DC and AC components of electric fields, the AC magnetic components of EM waves, and the energetic electron fluxes. The scientific payload, operated nearly continuously at magnetic latitudes below  $60^\circ$  over more than 6 years, has provided a very complete data set to monitor the mid and low latitude upper ionosphere on the night side of the orbit at a nearly constant local time between 21:30 and 22:30 LT. The scientific instruments were operated in high resolution *Burst* modes above seismic regions and lower resolution *Survey* modes elsewhere. The routine data processing provides the electron density  $N_e$  and temperature  $T_e$  from the Langmuir Probe Instrument (ISL) (Lebreton et al., 2006) with a time resolution of 1 s in both modes and the ion densities  $N_i$  and temperature  $T_i$  from the Plasma Analyzer Instrument (IAP) (Berthelier et al., 2006) with a time resolution of 2.2 s in *Burst* and 4.3 s in *Survey* modes. The solar and magnetic activities have been respectively defined by the *F10.7* index, measuring the solar flux at 10.7 cm, and the *Am* and *aa* usual global indices of magnetic activity.

## 3. Observations

Nguyen (2015) has performed a survey of the frequently observed plasma disturbances in the nighttime mid and low latitude ionosphere and put in evidence 5 different classes of events among which the most frequent, characterized by quasi-periodic fluctuations of the  $O^+$  ion density along the orbit track, has been identified as the signatures of MSTIDs.

Figure 1 shows, for the 2 December 2009 nighttime half-orbit 28,992\_1, an example of the orbit profiles of the ionospheric plasma parameters (electron density  $N_e$  and temperature  $T_e$ ,  $O^+$ ,  $H^+$ ,  $He^+$  densities) obtained from the routine level 1 data processing that constitute the basic data set of our study. During nighttime half-orbits, DEMETER travels from South to North and, within the time intervals highlighted in light blue, quasi-periodic variations of  $N(O^+)$  are present with amplitudes that may reach large levels up to 30%–50% of the undisturbed level. One may notice that the measured values of  $N_e$  are often larger than those of  $N(O^+)$ : this difference arises from two instrumental effects. Non uniformity of the surface properties of the ISL Langmuir probe have consistently altered the shape of the I/V characteristics, leading to 10%–15% overestimated  $N_e$  values retrieved from the routine processing algorithm. In addition, the DEMETER floating potential is often slightly positive, in particular

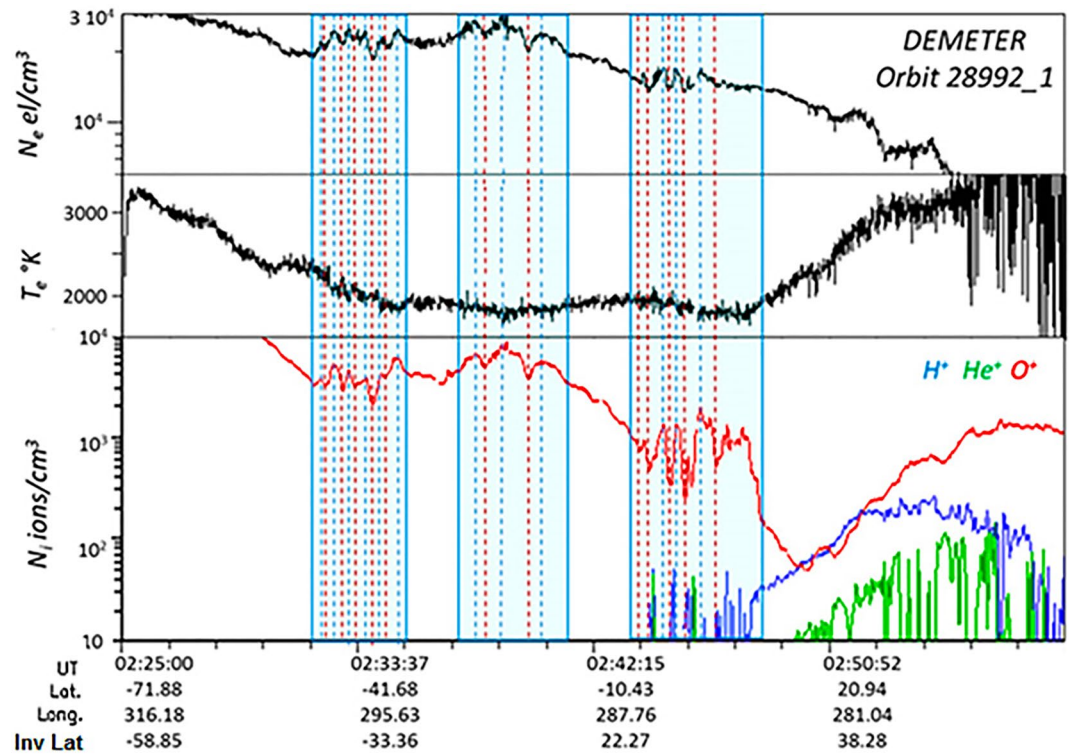


**Figure 1.** Nighttime half-orbit 28,992\_1, 2 December 2009. Orbit profiles of electron density  $N_e$ , electron temperature  $T_e$ ,  $H^+$ ,  $He^+$ ,  $O^+$  ion densities. Typical quasi-periodic variations of  $N(O^+)$  and  $N_e$  are observed in 3 time intervals highlighted in blue at 02:31.50–02:35.20 UT, 02:37.15–02:41.10 UT and 02:43.25–02:48.30 UT.

at low plasma densities, ranging from  $\sim 0.3$  to  $\sim 0.7$  V which prevents part of the light  $H^+$  ion distribution from being detected by the IAP ion analyzer. Since  $H^+$  ions have often densities of the same order of magnitude as  $O^+$  ions and may even be the dominant species in the mid-latitude nighttime topside ionosphere at the 650 km DEMETER altitude, missing  $H^+$  ions prevents a reliable measurement of the total ion density as is the case in the initial part of this half-orbit.

The data shown in Figure 1 are quite interesting since 3 different events have been detected. During the most intense one, from 02:43:35 to 02:48:30 UT at northern invariant latitudes between  $\sim 25^\circ$  and  $\sim 35^\circ$ , large amplitude oscillations of  $N(O^+)$  from  $\sim 3 \times 10^2$  ions/cm<sup>3</sup> to  $\sim 1.4 \times 10^3$  ions/cm<sup>3</sup> are observed together with oscillations of  $N_e$  and faint ( $< 100$  K) anti-correlated  $T_e$  variations. In the opposite hemisphere, an event occurs between 02:31:50 and 02:35:20 UT, at southern invariant latitudes between  $\sim 40^\circ$  and  $\sim 25^\circ$ , with smaller amplitude oscillations of  $N(O^+)$  and  $N_e$  and similarly anti-correlated  $T_e$  variations of  $\sim 100$ – $150$  K. In addition, a third event is observed between 02:37:15 and 02:41:10 UT, extending across the magnetic equator between invariant latitudes  $\sim -12^\circ$  in the South and  $\sim +15^\circ$  in the North, with 3 maxima in  $N(O^+)$  and  $N_e$  yet at larger distances from each other than the successive maxima in the two previous events and with no detectable variations of  $T_e$ .

## 4. MSTID Detection and Data Analysis

### 4.1. MSTID Detection

MSTID events have been detected by Nguyen (2015) through a visual analysis of the IAP thermal ion density profiles along night time orbits. Based on electron density  $N_e$  observations reported in previous studies (e.g., Park et al., 2010; Shiokawa, Ihara, Otsuka, Ogawa, et al., 2003), a “guiding model” of the main features of these events was established to allow their reliable recognition and detection. Basically, MSTIDs are recognized from the occurrence of quasi-periodic fluctuations of the  $O^+$  ion density  $N(O^+)$  superimposed on a rather continuous large scale profile and lasting more than 1 min in spacecraft time that is,  $\sim 450$  km along the DEMETER orbit. This later criterion allows to sort out short duration ionospheric disturbances of different origin while the



average duration of MSTID events ranges from  $\sim 3$  to 5 min in spacecraft time. This simple guiding model fully corresponds to MSTID features reported in several more recent studies for example, Kil and Paxton (2017), Lee et al. (2021).  $O^+$  ion density data were considered for MSTID detection because the relative fluctuations of  $N(O^+)$  are larger than those of light ion and electron densities thus allowing a more sensitive and reliable detection. This stems from the initiation of MSTIDs in the bottom-side ionosphere where  $O^+$  is the by far the dominant ion species on which are set-up the plasma disturbances and also, as shown in Park et al. (2010), from the smaller  $O^+$  scale height compared to that of light ions or  $N_e$ . Due to the  $\sim 4$  eV ram energy of  $O^+$  ions, their measurement by the IAP analyzer are not impeded by a  $\leq 1V$  positive spacecraft potential, making their orbit profiles free from the spacecraft potential variations.

At low latitudes, Equatorial Plasma Bubbles (EPB) are also regularly observed on data from the DEMETER plasma instruments IAP and the Langmuir probe ISL. Due to the 21.30–22.30 local time interval of DEMETER night time orbits, EPBs are in their early stage of development, with a rather moderate drop in the mean plasma density compared to the fully developed events after midnight. They bear some resemblances with MSTIDs, which may arise in part from common triggering mechanisms associated with AGW. In order to distinguish these two classes of events, another simple guiding model was established for the EPB based on two main features of the  $N_e$  and  $N(O^+)$  profiles: (a) a decrease of the mean  $N_e$  and  $N(O^+)$  values by at least a factor 2 compared to the undisturbed level before and after the EPB, (b) a rather fast drop of  $N_e$  occurring in less than 15s spacecraft time at the start or end of the event or both, easily observed thanks to the 1s time resolution of  $N_e$  measurements.

The visual detection performed by Nguyen (2015) certainly required more work and longer efforts than the automatic detection of MSTID's solely based on the level of  $N_e$  fluctuations often used in previous studies. However, it offers definite advantages for a reliable and accurate MSTID detection clearly distinguished from EPBs for which a data base of high interest is also obtained.

#### 4.2. Data Processing

To perform the data analysis independently of the actually operated *Burst* or *Survey* modes the  $N(O^+)$  and  $N_e$  densities measurements were re-sampled by a simple linear interpolation at a common time resolution of 4 s. From the initial visual examination of the  $N(O^+)$  orbit profiles, approximate *Start* ( $T_1$ ) and *End* ( $T_2$ ) times are defined for each event and registered in an event database. The ensuing data processing includes 4 steps:

- *Step 1:* Determination of the undisturbed base line  $P(t)$  of  $N(O^+)$  that would be observed in absence of disturbances. To this aim, a time interval  $[T_A, T_B]$  encompassing the event is considered by taking into account 32 undisturbed data points (128 s) before  $T_1$  (in the time interval  $[T_A, T_1]$ ) and 32 undisturbed data points after  $T_2$  (in the time interval  $[T_2, T_B]$ ) to compute a weighted fit of  $N(O^+)$  in the interval  $[T_A, T_B]$  based on a 7th degree polynomial expansion. Data points within the undisturbed intervals  $[T_A, T_1]$  and  $[T_2, T_B]$  are given 5 times larger weight than data points within  $[T_1, T_2]$ . This method was validated on several orbits with no events to ensure that  $P(t)$  matches the measured  $N(O^+)$  profile in the interval  $[T_A, T_B]$ .
- *Step 2:* Accurate determination of the actual start  $T_d$  and end  $T_f$  times. The standard deviation  $Std$  of the differences between the data points and  $P(t)$  is computed over 8 data points (i.e., 32 s) that are successively moved forward by two points (i.e., 8 s) in order to smooth the standard deviation variations while maintaining a sufficient time resolution. The average value  $Stdref$  of the  $Std$  values computed for the 8 first and 8 last intervals, that is, well before and after the event, is taken as a reference of the background fluctuations in the undisturbed ionosphere. Then, starting at the end of the last reference interval before the event, the exact *Start time*,  $T_d$ , is defined as the mean time of the first segment of eight points when  $Std$  exceeds  $1.5 * Stdref$ . Similarly, the exact *End time*,  $T_f$ , is the mean time of the last segment of eight points when  $Std$  is larger than  $1.5 * Stdref$ .
- *Step 3:* Normalization of the  $N(O^+)$  variations. The relative differences  $d(t) = (N(O^+) - P(t)) / P(t)$  characterizes the instantaneous relative amplitude of the disturbances and allows comparing events irrespective of the actual mean value of  $N(O^+)$  which is subject to large day-to-day, seasonal and solar cycle variations.
- *Step 4:* Computation of the frequency power spectrum of the normalized differences  $d(t)$ . In order to limit the frequency leakage due to time domain truncation, a Hanning truncation function was applied on  $d(t)$  in the interval  $[T_A, T_B]$  to get the windowed signal  $\delta(t)$  before computing the FFT (Brigham, 1974). The FFT provides the frequency spectrum of the normalized  $N(O^+)$  variations along the orbit. The lowest frequency range  $F \leq F_{min} \approx 1.5 / (T_f - T_d)$  must be discarded since this part of the spectrum cannot be properly evaluated using the simple FFT and would require a more sophisticated technique such as wavelet transform. Owing

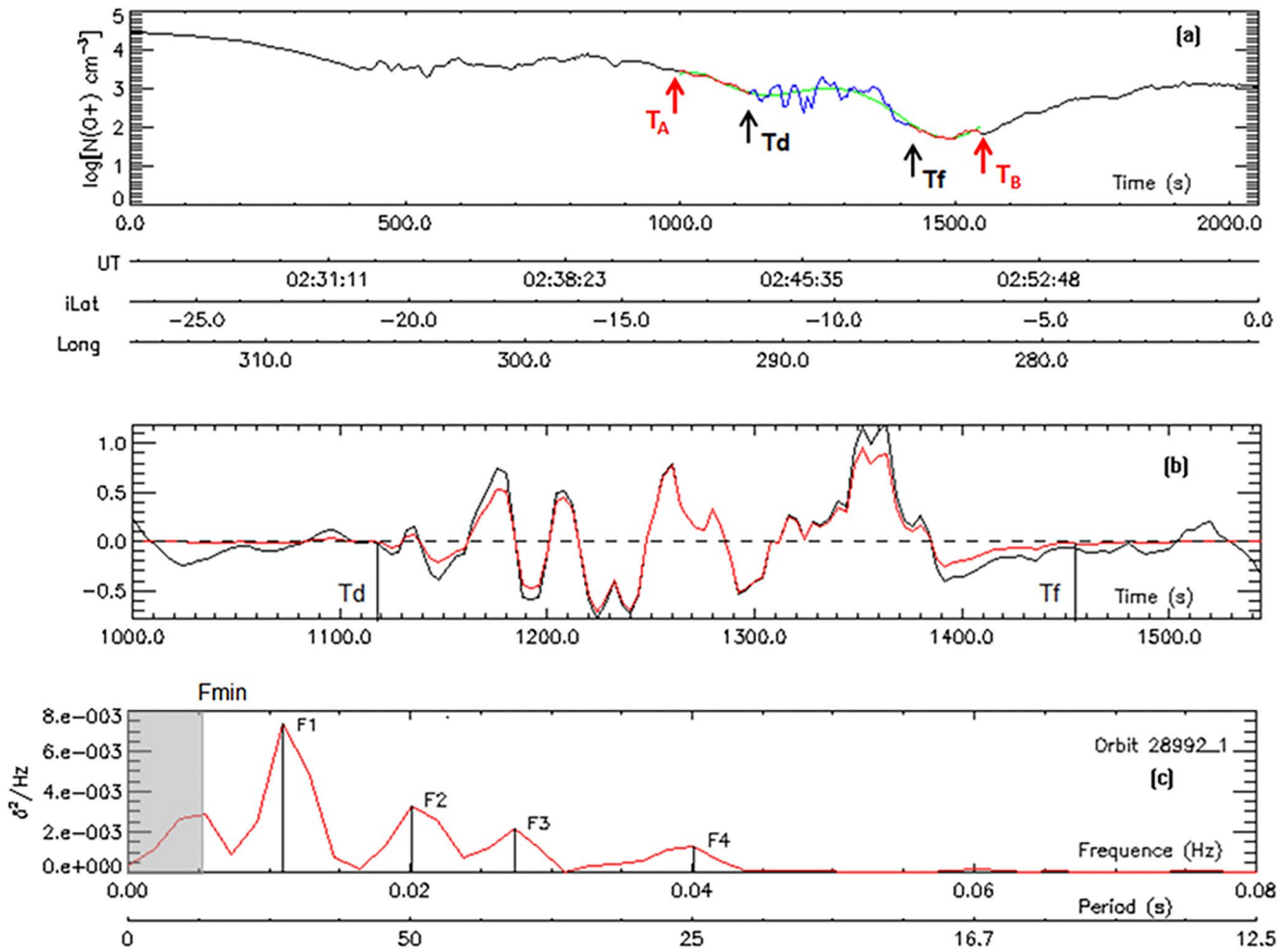


**Figure 2.** Illustration of the data processing for orbit 28,992\_1. (a): Orbit profile of the  $O^+$  ion density  $N(O^+)$ , shown in blue during the visually detected event duration, in red the two 128s extended periods before and after the event used to derive the base line through a fit by a 7th degree polynomial function  $P(t)$ . The accurate start and end times,  $T_d$  and  $T_f$ , determined by the method described in the text are indicated by arrows. (b): Normalized disturbance  $d(t) = [(N(O^+)(t) - P(t))/P(t)]$  (black curve) and  $\delta(t)$  normalized disturbance after windowing by a Hanning function in the extended interval  $[T_A, T_B]$  (red curve). (c): Frequency power spectrum of the windowed signal. The gray area corresponds to the frequency range below  $F_{min}$ , not to be taken into account as indicated in the text.

to the DEMETER orbital velocity of  $\sim 7.3$  km/s, much larger than the development rate of MSTIDs and their own maximum propagation velocity less than  $\sim 150$  m/s (Otsuka et al., 2021), the  $N(O^+)$  profile retrieved from DEMETER measurements provides a quasi-instantaneous image of the spatial structures of the MSTIDs encountered along the orbit. Therefore, the “frequencies” in the spectra can be interpreted in terms of “spatial periods” or “spatial wavelengths” of the ionospheric disturbances along the orbit.

### 4.3. Example

The three panels in Figure 2 display results from the data processing in the case of the major event in half-orbit 28,992\_1 in the time interval 02:43:35–02:48:30 (see Figure 1).

Panel (a) shows the  $N(O^+)$  profile in the half-orbit, shown in blue between  $T_1$  and  $T_2$ , in red in the extended intervals  $T_A T_1$  and  $T_2 T_B$  with the base line  $P(t)$  between  $T_A$  and  $T_B$  drawn in green. In the  $T_A T_1$  and  $T_2 T_B$  intervals of time corresponding to the undisturbed ionosphere before and after the MSTID, the base line  $P(t)$  reproduces nearly perfectly the measured  $N(O^+)$  profile and, at the scale of the Figure, practically no differences between these two curves can be seen so that the measured  $N(O^+)$  profile in red masks the green base line curve. The accurate *Start* and *End* times,  $T_d$  and  $T_f$ , are indicated by arrows. Panel (b) displays a zoomed view of the measured and windowed  $N(O^+)$  profiles during the event with the computed start ( $T_d$ ) and end time ( $T_f$ ). Large quasi-periodic

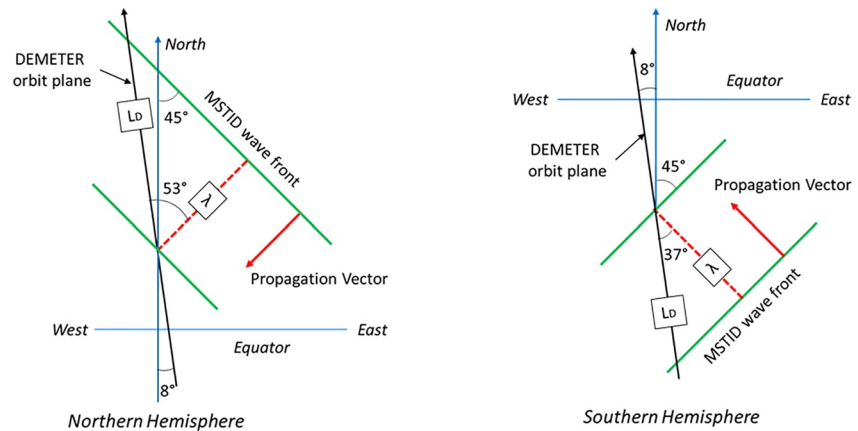


**Figure 3.** Derivation of the actual Medium-scale traveling ionospheric disturbances wavelength from the along orbit assuming that the propagation velocity is along the average direction, toward SW in the Northern hemisphere and NW in the Southern hemisphere.

variations of  $N(O^+)$  are observed up to  $\sim 50\%$  of the background level. In panel (c) the power spectrum exhibits four peaks at frequencies well above the frequency range below  $F_{\min}$  highlighted in light gray and with similar FWHM of  $\sim 0.005$  Hz. At  $F_1 \sim 0.0109$  Hz the peak power is  $P_1 \sim 7.510^{-3}$  in  $\delta^2/\text{Hz}$ , at  $F_2 \sim 0.021$  Hz,  $P_2 \sim 3.10^{-3}$  and at  $F_3 \sim 0.0275$  Hz,  $P_3 \sim 2.10^{-3}$ . Even if part of the power in the second peak near 0.022 Hz may arise from the first harmonics of the first peak due to the sharp gradients in the large  $N(O^+)$  increase at the beginning of the event, a detailed examination of the density profiles of panel (b) shows that the  $F_2$  and  $F_3$  peaks mainly represent the actual quasi-periodic variations of  $N(O^+)$  close to these frequencies. The last smallest peak at  $F_4 \sim 0.04$  Hz has a slightly wider FWHM. As seen on Figure 2 the faster quasi-periodic fluctuations responsible for the  $F_4$  peak mainly occur during limited time intervals [1220–1250] and [1320–1370] which may explain its slightly wider FWHM.

Most power spectra display a sequence of several peaks with decreasing amplitudes at higher frequencies similar to the example shown in Figure 2. Some events are characterized by a power spectrum with a single peak, implying that, in such situations, plasma oscillations develop at a rather sharply defined frequency. The main peak at the lowest frequency may arise from the existence of a large disturbance in the  $N(O^+)$  orbit profile usually observed at the beginning or end of the event, possibly a remnant of the initial triggering disturbance. The following peaks with smaller amplitudes are representative of the quasi-periodic oscillations actually observed during the main part of the event and related to the local ionospheric instability. Sharp gradients are often observed on the flanks of the large  $N(O^+)$  disturbance and may reflect non-linear physical processes involved in the MSTID evolution and propagation. These sharp gradients generate harmonic frequencies in the power spectra but, as already mentioned for the power spectrum in Figure 2, the tests performed on a number of events have shown that these harmonics contribute for a minor part to the peaks at higher frequencies in the spectrum that are thus representative of actual plasma oscillations. A more extensive analysis of the power spectra and their variability is foreseen in a forthcoming paper.

#### 4.4. MSTID Wavelengths and Power Spectra

Typical wavelengths of MSTIDs determined from optical observations range from 50 to 500 km over Arecibo (Garcia et al., 2000) and from 100 to 300 km in the Japanese sector (Shiokawa et al., 2002) while Valladares and Hei (2012) reported average wavelengths on the order of 450 km from TEC measurements over Peru. Altogether, an average range of  $\sim 50$ –600 km appears statistically relevant for MSTIDs. Although noticeable differences may exist among individual events, ground-based observations have shown that, on the average, MSTIDs are elongated along a NW-SE direction and move toward SW in the Northern hemisphere with a configuration symmetrical with respect to the equator for events occurring in the Southern hemisphere. Since the orientations of MSTIDs cannot be retrieved from the  $N(O^+)$  orbit profiles alone, we have assumed that, in all cases, they follow the average NW-SE orientation and move in the perpendicular SW direction. As illustrated by the two sketches in Figure 3, drawn in geographical coordinates respectively for the Northern and Southern hemispheres, the



relations between the measured spatial period  $L_D$  along the DEMETER orbit and the actual MSTID wavelength  $\lambda$  perpendicular to the front direction are as follows:

$$\lambda \sim 0.6L_D (\text{Northern hemisphere}) \text{ and } \lambda \sim 0.8L_D (\text{Southern hemisphere}) \quad (1)$$

Due to the very crude assumptions underlying these relations, we took as a realistic average estimate  $\lambda \sim 0.7L_D$  with an uncertainty of  $\sim \pm 0.1L_D$ . Occurrence maps presented in Section 5 show that MSTIDs are organized with respect to the Earth's magnetic field, thus the orientation and propagation direction of the MSTID should also be evaluated in a frame of reference linked to the Earth's magnetic field. In the Pacific sector, where MSTID occurrence maximizes, the Earth's magnetic field meridians are inclined by  $\sim 6\text{--}7^\circ$  with respect to the geographic equator thus the  $37^\circ$  angle for the Southern hemisphere in Figure 3 would be increased to  $\sim 43^\circ$  and the relation (Equation 1) would be  $\lambda \sim 0.73L_D$  thus slightly closer to the adopted relation  $\lambda \sim 0.7L_D$ .

For a spectral peak at frequency  $F_i$ , the corresponding spatial period  $L_D$  along the orbit is  $L_D(\text{km}) = 7.3/F_i(\text{Hz})$  and the estimated MSTID wavelength  $\lambda(\text{km}) \sim 5.1/F_i(\text{Hz})$  with an uncertainty of  $\pm 0.7/F_i(\text{Hz})$ . Taking 600 km as a maximum value for the MSTID wavelengths leads to a threshold value of  $F_L \sim 0.008 \pm 0.001$  Hz for the lowest frequency peak in the spectra.

A preliminary survey of power spectra disclosed only occasional cases with a first peak at a frequency  $F_p < F_L$ . As mentioned in the previous paragraph, this may arise (a) from a specific MSTID configuration with a very large disturbance at the beginning or end of the event yet showing several large enough peaks at higher frequencies or (b) from the erroneous detection of a Large Scale Traveling Ionospheric Disturbances (LSTID). To eliminate those very rare LSTID events we have applied the following criteria: an event was considered as a MSTID (a) if  $F_p \geq F_L$  or (b) if  $F_p < F_L$  but the spectrum includes a peak at a frequency  $F > F_L$  with a power at least 20% of the power of the first peak. It must be pointed out that only very few detected events were considered as non-MSTID events and rejected, which attests of the effectiveness of the visual detection procedure.

## 5. Main Statistical Features of MSTIDs

The main statistical features of the MSTIDs detected from the DEMETER database, such as their geographical distribution, dependence on solar and magnetic activity, seasonal variations, are reported in this section. A more detailed analysis and discussion of the inter-annual and seasonal variations is given in Section 6.

One of the main advantage of DEMETER observations stems from the 6 years long homogeneous set of measurements gathered at a nearly constant altitude (710 km the first year, then 650 km) over all longitudes at magnetic latitudes less than  $60^\circ$  and, on the night side part of the orbit, at a practically constant local time of  $22.00 \pm 0.5$  hr. This avoids in particular the necessity to disentangle local time from longitude and seasonal variations, often an issue for satellite observations. Also, and more importantly, this large database encompasses the declining phase of solar cycle 23, the deep solar minimum of 2008–2009 and the early rise of solar cycle 24, thus providing detailed insights on the influence of solar activity on MSTID seasonal variations and geographic distribution.

### 5.1. Quantitative Comparison of DEMETER Occurrence Rates With Previous Observations

Before discussing the main outcomes of our study, we have first ascertained our results by checking that the DEMETER occurrence rates are consistent with those derived from ground-based or other satellite observations at similar locations and time periods. To compare with optical imager observations, our data were averaged over an area commensurate with the imager FOV using information given by Duly et al. (2013). Optical imagers used for MSTID observations are typically all-sky cameras with a fisheye lens and an optics, possibly with various filters allowing to observe different line emissions, coupled to a Charge Coupled Device. From long duration observations at  $15^\circ\text{S}$  magnetic latitude in Brazil, Amorim et al. (2011) reported occurrence rates of 28% and 20% in 2007 and 2008, in good agreement with the corresponding 31% and 18% DEMETER values. Average values derived from the CASI imager data at Hawaii ( $20^\circ\text{N}$ ) by Duly et al. (2013) in 2007–2009 amount to  $\sim 60\%$ , about 12% larger than the corresponding DEMETER values. This difference can be explained by the early evening DEMETER orbit while CASI operates over the entire night and MSTID activity is known (Amorim et al., 2011) to maximize in the 23–02 LT interval especially during periods of low solar activity. Our  $\sim 40\%$  occurrence rates over China in 2009 are larger than the 30% values deduced from TEC measurements using a cluster of GPS

stations in the Hubei region (29°–33°N) by Ding et al. (2011). This difference is likely explained by a higher efficiency of visual detection by a trained observer of distinct  $N(O^+)$  undulations on DEMETER measurements compared to the complex processing algorithms of TEC maps with safe enough thresholds to avoid false detection and also by the possibly degraded TEC measurement when the line of sight is not parallel to wave-fronts.

DEMETER occurrence rates are generally comparable and slightly larger than those derived from KOMPSAT and CHAMP (Park et al., 2010, 2015). CHAMP, at 400 km altitude, is closer to the 250–300 km altitude range where MSTIDs start to develop, thus could be thought in a mode favorable position to detect newly formed MSTIDs. As mentioned just above, visual detection certainly offers a higher capability to recognize the MSTIDs than the automatic detection of  $N_e$  fluctuations used by Park et al. (2010). Yet, another reason may play a major role to explain the observed counter-intuitive difference between DEMETER and CHAMP observations. At the 650 km altitude of DEMETER, the  $N(O^+)$  scale height is smaller than the  $N_e$  scale height at CHAMP so that, as shown by Park et al. (2010), the relative variations of  $N(O^+)$  with respect to background are larger than those of  $N_e$ , making therefore the recognition of weak events easier and offering a more sensitive detection of MSTIDs on DEMETER  $N(O^+)$  data.

## 5.2. Average Geographic Distribution and Main Regions of Occurrence

MSTIDs are mainly observed at mid-latitudes, in accordance with the physical processes involved in their development mainly based on the existence of structured electric fields associated with Es layers, as already mentioned in the Introduction. This is easily recognized on Figures 4a and 4b where are displayed the orbit segments along which MSTIDs were detected for 2 representative years, 2007 with the largest annual occurrence rate and 2009 during the deep solar minimum with a smaller occurrence rate.

These Figures also show that a number of events occur at magnetic latitudes less than  $\sim 15^\circ$ , considered in earlier studies (Shiokawa et al., 2002) as the average low latitude boundary of MSTIDs. These observations will be discussed in more details in the following paragraph Section 5.3.

Maps of the average annual occurrence rates with a pixel size of  $10^\circ$  in longitude and  $5^\circ$  in latitude summarize the main features of the MSTID geographic distribution in each of the 6 years of DEMETER operation from 2005 to 2010.

For a given pixel the occurrence rate is defined as the ratio between the number of orbit segments crossing this pixel along which an event was detected and the total number of orbit segments that cross this pixel. These maps extend those previously presented by Park et al. (2010) based on electron density measurements from CHAMP, KOMPSAT and DMSP, for shorter periods in 2000–2001 (high solar activity) and 2006–2007, and put in evidence new findings, in particular during the deep solar minimum when Northern MSTIDs occur more frequently than Southern ones. MSTIDs develop mainly over approximately conjugate areas between  $\sim 10^\circ$  and  $\sim 45^\circ$  latitudes in each hemisphere in accordance with several case studies reported from coordinated ground-based campaigns (Martinis et al., 2019; Otsuka et al., 2004; Shiokawa et al., 2005) and satellite observations (Burke et al., 2016). On the average MSTIDs occur more frequently in the Southern hemisphere ( $\sim 41\%$  average occurrence rate) than in the Northern hemisphere ( $\sim 26\%$ ) with an average South/North ratio of  $\sim 1.6$ , except in 2009 when this ratio falls to  $\sim 0.9$  with Northern more frequent than Southern MSTIDs. Occurrence rates reach their largest values in the  $110^\circ$ – $300^\circ$  longitude Southern sector from Australia to South America, in particular in 2006 and 2007, with localized enhancements observed in the Central Pacific area and close to South America. Specific conditions and/or physical processes in the ionosphere and upper atmosphere should combine in this longitude sector to favor the instability that allow MSTIDs to develop while they are not met over Europe and Africa. The regular existence of AGW generated over the Andes mountains (e.g., Hoffmann et al., 2013), ultimately propagating into the lower thermosphere, might be of importance for the generation of instabilities leading to the development of MSTIDs. In 2006–2007, enhanced occurrence rates, yet at a lower level, are also observed in the North over the same longitude sector, encompassing China, Japan and the Pacific Ocean while they are significantly lower over Europe and Africa with a clear minimum around the South Atlantic Anomaly. Due to the wide spread oceanic areas in the Southern hemisphere, few ground-based studies allow only a partial comparison with satellite results. Using GPS/TEC measurements in 1998–2001, Kotake et al. (2006) derived regional MSTID activity indices over 6 areas in the East and West coasts of Northern America, South America, Europe, Japan and Australia, showing a minimum over Europe and a maximum over Japan and Australia, in good agreement with our maps. Following

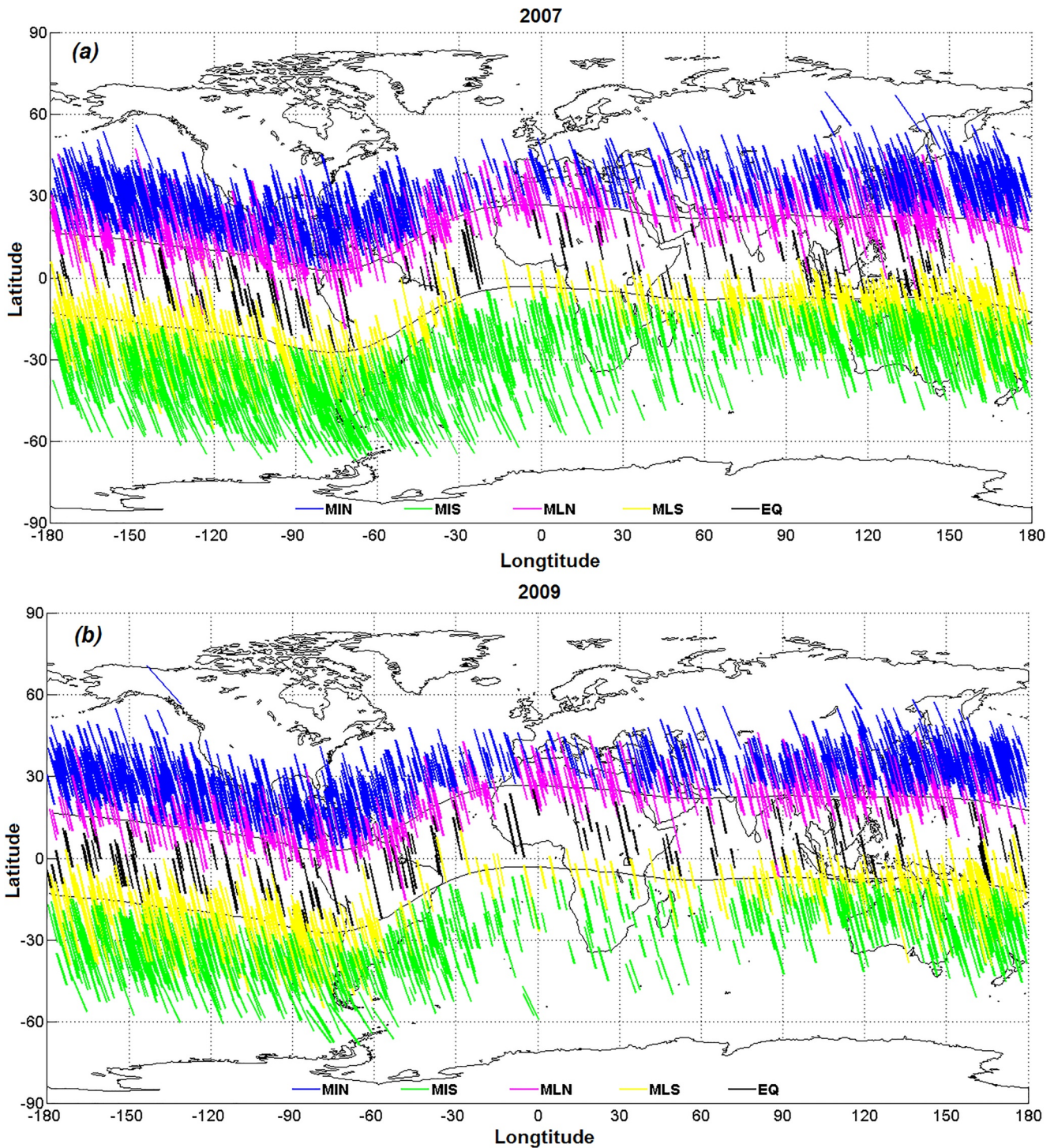


**Figure 4.** *4a* in 2007, *4b* in 2009. Segments of orbit tracks where a Medium-scale traveling ionospheric disturbances was detected. Indicated are the Northern and Southern lines of 15° magnetic latitude defining the equatorial belt discussed in the text. MIN (in blue) and MIS (in green) occur only at mid-latitudes, respectively in the Northern and Southern hemispheres. MLN (in purple) and MLS (in yellow) extend mainly at mid-latitudes and partly within the equatorial belt, respectively in the Northern and Southern hemispheres. EQ (in black) occur only in the equatorial belt (see Section 5.3 for more detailed definitions).

the decrease of solar activity between 2005 and 2007, occurrence rates increase and the latitudinal extent of the MSTID area broadens, in particular in 2007. During the deep solar minimum of 2008 and 2009 two noticeable differences are observed. The clear global minimum of occurrence in 2008 is opposite to the increasing



occurrence rates between 2005 and 2007 a period when the solar activity was already decreasing. This is also contradictory to previously published results and model predictions of more favorable ionospheric conditions for MSTID development during periods of low solar activity. In 2009 MSTIDs are more frequent in the Northern hemisphere than in the Southern hemisphere with a maximum of  $\sim 35\%$  over the South-Asia and Japan  $130^\circ$ – $210^\circ$  longitude sector. These two new findings are related to modifications of the seasonal variations which will be discussed in more detail in Section 6.

### 5.3. Low-Latitude MSTIDs

Low latitude MSTIDs have been recently reported by Figueiredo et al. (2018), and Sivakandan et al. (2019). We have taken advantage of the long duration of DEMETER observations and the large number of events in our data base, to assess the occurrence of MSTIDs at low latitudes in more detail. To this aim, as suggested by Shiokawa et al. (2002), we took  $+15^\circ$  and  $-15^\circ$  as the low magnetic latitude boundaries of the truly mid-latitude MSTIDs, and sorted the MSTID events among 5 categories that can be easily recognized in Figures 4a and 4b.

- MIN and MIS occur only at mid-latitudes, external from the  $-15^\circ$  to  $+15^\circ$  latitude range of the so-called “equatorial belt.”
- MLN and MLS extend mainly at mid-latitudes and partly within the equator belt below  $\sim 15^\circ$  latitude respectively in the Northern and Southern hemispheres
- EQ occur only in the equatorial belt at magnetic latitudes lower than  $15^\circ$ .

The following conclusions can be drawn:

- Although low ( $<15^\circ$ ) invariant latitude MSTIDs are much less frequent than those present at mid-latitudes, there is a clear evidence that MSTIDs are observed at low latitudes, even across the magnetic equator, with MLS and MLN often extending to latitudes lower than  $\sim 10^\circ$ .
- The relative annual occurrence rates of the 5 categories stay rather similar over the whole period of DEMETER observations 2005 to 2010 and are not affected by the varying solar activity.
- MLS occur more frequently than MLN, as is the case of MIS versus MIN illustrated by Figure 5.
- MLN and MLS events have wavelength and amplitudes similar to MIS and MIN events and appear as mid latitude MSTIDs that found proper conditions in the ionosphere and thermosphere to propagate down to low latitudes (Lee et al., 2008). It is generally thought that the low latitude extent of MSTIDs is limited by the Equatorial Ionization Anomaly (EIA) where higher plasma density and ion-neutral collision rates damp the ionospheric instability which triggers the MSTID development. Conditions allowing MSTIDs to propagate to low latitudes are encountered for weakly developed EIA as may be more often the case during solar minimum (Makela et al., 2010).
- A distinct feature, clearly seen on the two maps in Figures 4a and 4b, is the existence of truly Equatorial Events (EQ), close to or over the magnetic equator. They usually extend only  $\sim 7^\circ$ – $10^\circ$  in latitude along the DEMETER orbit, hence over shorter distances than mid-latitude events, yet exhibiting similar characteristics in wavelength and amplitudes. Only sparse observations of very low latitude MSTIDs have been previously reported, all from optical ground-based observations: over Chili down to  $\sim 5^\circ$ S magnetic latitude by Makela et al. (2010), over the Malaysian peninsula  $\sim 5^\circ$  north of equator by Husin et al. (2011), at the magnetic equator (magnetic latitude  $\sim 0.5^\circ$ N) in Brazil by Paulino et al. (2016) and more recently over India down to  $\sim 3.5^\circ$  magnetic latitude by Sivakandan et al. (2019). The  $\sim 3\%$  average occurrence rate of our EQ events is similar to those reported by Husin et al. (2011). The origin of equatorial MSTIDs has been questioned since both the nearly horizontal Earth's magnetic field and the extremely seldom detection of *Es* layers in the equatorial regions make unlikely their local generation through the *Es-F* region coupling mechanism (Tsunoda & Cosgrove, 2001) effective at mid-latitudes. Nevertheless, Makela et al. (2010) and Sivakandan et al. (2019) ascertained the existence of electrified MSTIDs in their observations and suggested they may be initiated at mid-latitudes and further drift toward equatorial regions whenever they meet favorable conditions in the ionosphere. On the other hand, Paulino et al. (2016) concluded from their observations that MSTIDs were different in nature and took their origin from the upwards propagation of AGW interacting with the ionospheric plasma but the physical processes that could account for their development and evolution have yet to be fully demonstrated by theoretical investigations and numerical models. Some of our EQ events extend till the  $15^\circ$  boundary and may well correspond to the events of the first type, while isolated ones with a reduced extent

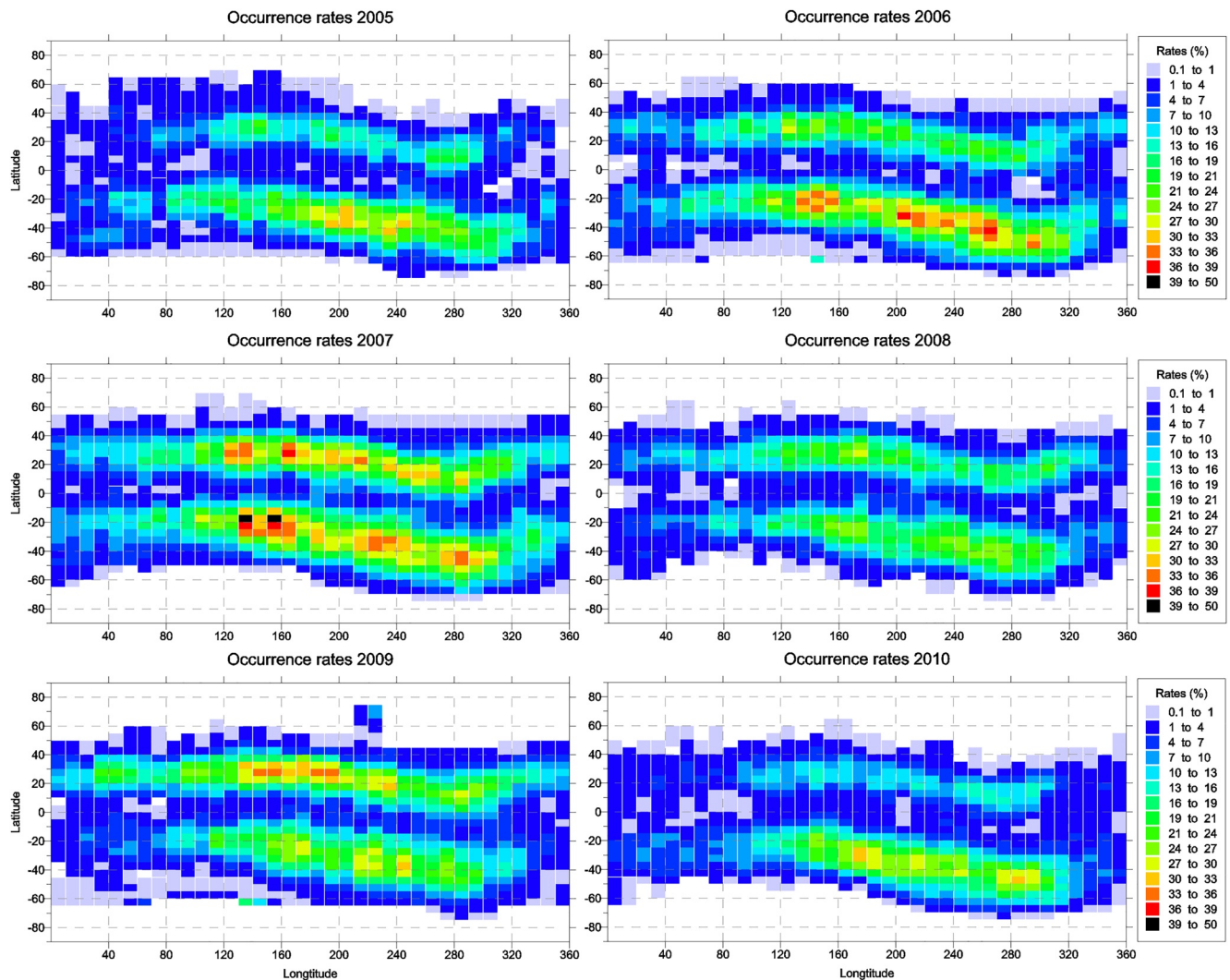


**Figure 5.** Geographical maps of the annual averages of Medium-scale traveling ionospheric disturbances occurrence rates from 2005 to 2010. Pixels: 10° in longitude, 5° in latitude.

along the orbit may belong to the second type. A more detailed investigation of the EQ events, taking into account additional measurements onboard DEMETER, will be subject of a future study.

#### 5.4. Dependence on Magnetic Activity

A separate analysis (not presented here) performed separately for the MIN and MLN (respectively MIS, MLS) events has shown that events of both categories respond similarly to magnetic activity. We have therefore drawn in Figure 6, for each year from 2005 to 2010, the average curves showing the occurrence rates of Northern (resp. Southern) mid-latitudes MSTIDs irrespective of their low latitude extent as a function of magnetic activity. A similar Figure is shown for EQ events that only occur within the “equatorial belt.” Each nighttime half orbit was characterized by the Am index of magnetic activity in the corresponding 3-hr interval and the occurrence rates were averaged for 6 classes of Am indices [0–10], [10–20], [20–30], [30–40], [40–60] and [>60]. The average occurrence rate in each class is defined as the ratio between the number of orbits with an event and the total number of orbits in this class.

As shown by Figure 6, the MSTID occurrence follows similar trends with respect to magnetic activity in both hemispheres: occurrence rates maximize during very quiet periods ( $A_m < 10$  nT) at ~15%–27% in the North and ~20%–35% in the South depending on solar activity, then decrease regularly when magnetic activity increases,



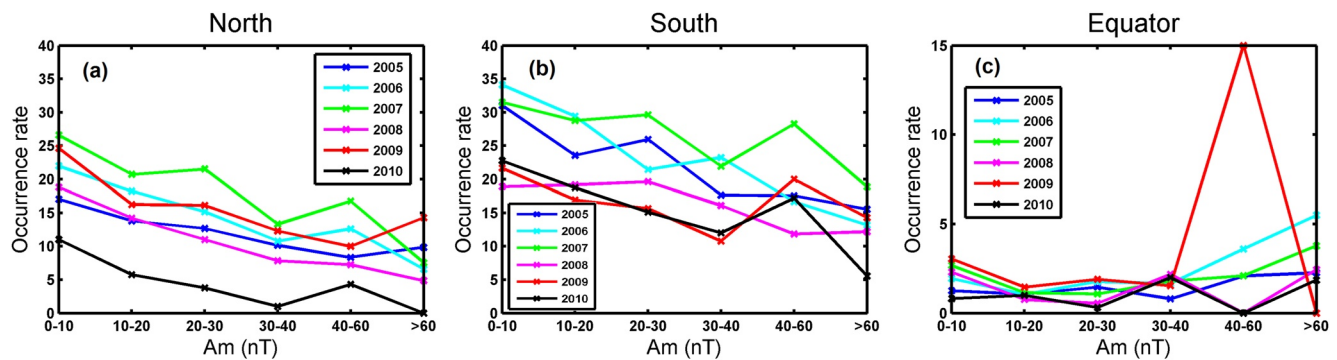


**Figure 6.** Variations of the Medium-scale traveling ionospheric disturbances occurrence rates as a function of the Am magnetic activity index shown separately for each of the 6 years 2005–2010, (a) Northern hemisphere events with a high magnetic latitude end  $>15^\circ$ , (b) Southern hemisphere events with a high magnetic latitude end  $<-15^\circ$ , (c) Equator events occurring at magnetic latitudes  $<15^\circ$ .

down to  $\sim 7\%$ – $15\%$  in the North and  $10\%$ – $20\%$  in the South for very active periods with  $A_m \geq 50$  nT. Based on TEC and optical observations Huang et al. (2016) found similar variations in 2013–2015 at Northern mid-latitudes in China, with a somewhat steeper decrease when magnetic activity increases since they did not detect any significant MSTID activity for  $K_p > 4$ . Their lower occurrence rate during disturbed periods may arise both from difficulties in distinguishing actual MSTID events from large TEC irregularities present during disturbed periods and from an already significant reduction of MSTID activity in 2013–2015, close to the maximum of solar cycle 24. Due to poor statistics the dependence of the occurrence of EQ events on magnetic activity cannot be accurately evaluated but it seems practically independent on magnetic activity except for a weak increase during very active periods ( $A_m \geq 50$  nT). This feature may indicate that, at least, part of the EQ events arise from the interaction of AGW with the ionosphere: large auroral events are indeed known to be a major source of high altitude AGW that propagate from the mid-latitude heated thermosphere toward equatorial regions. The anomalous peak observed in 2009 for a large enough magnetic activity ( $40 < A_m < 60$  nT) is correlated with a similar peak of Southern mid-latitude MSTIDs although, on the average, Northern events predominate during the same period as evidenced by Figure 5.

Magnetic activity is a reliable image of auroral activity which is known to be a source of AGW from the lower thermosphere heating by precipitating auroral particles. AGW propagate toward lower latitudes and have been invoked as a possible seeding mechanism for MSTIDs: the anti-correlation between MSTIDs and magnetic activity clearly shows that, in practice, this mechanism is superseded by other physical processes that counteract the development of MSTIDs. Two different phenomena may be suggested. First, the mid-latitude thermosphere heating associated with auroral events, enhances the ion-neutral collision frequency and the integrated Pedersen conductivity in the lower F-region, leading to a substantial decrease of the Perkins instability growth rate. In addition, large-scale electric-fields are induced in the mid-latitude nighttime ionosphere by the extension of the auroral zone to lower latitudes and the intensified auroral convection: they may modify the pre-existing electric field patterns associated with  $E_s$  layers, leading to inadequate conditions for the development of electrified MSTIDs.

The statistical anti-correlation of MSTIDs with magnetic activity may also be observed on temporal sequences as illustrated in Figure 7 for April 2010. The  $A_m$  magnetic activity index is shown by the blue curve and MSTIDs are indicated by bars, red in the North, green in the South, with the height of each bar proportional to the amplitude of the main peak in the frequency power spectrum above  $\sim 0.011$  Hz (see Section 4) representative of the amplitude of the quasi-periodic oscillations of  $N(O^+)$ . A CME hit the Earth on April 5 at 08.25 UT, followed by high speed solar wind streams flowing from a coronal hole observed by SOHO (Fathy et al., 2014; Shmeis et al., 2012). The  $A_m$  magnetic activity index peaks at  $\sim 60$  nT on days 5 and 6, decreases to moderate values between 20 and 30 nT in days 10–15 and to rather small values till the end of the month except between days 22 and 24 where  $A_m$  rises again to  $\sim 15$  nT. The number and amplitude of MSTID events are much larger in the Southern hemisphere, illustrating the general predominance of Southern events, and maximize in the second half of the month with a lack of events on day 12 simultaneously with the 30 nT peak of  $A_m$  on the same day and, similarly, a lack of events on day 15 following the rise of  $A_m$  to 15 nT on day 14. In the remaining of the month,

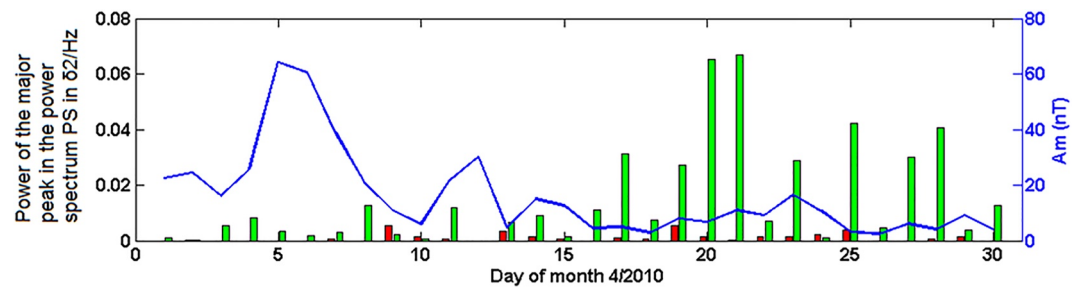


**Figure 7.** A real-time evidence of the effect of magnetic activity on the occurrence of Medium-Scale Traveling Ionospheric Disturbances during April 2010: few events during the disturbed first 15 days, a large number of events during the quieter last 15 days.

as soon as the activity drops, the amplitude and number of MSTIDs increase as exemplified during days 13 and 14 and days 16–20.

### 5.5. Solar Activity and MSTID Occurrence

The anti-correlation between solar activity and MSTIDs has long been reported (e.g., Candido et al., 2008; Kotake et al., 2007; Shiokawa, Ihara, Otsuka, & Ogawa, 2003) and shown in more details by a recent study focused on the Japan longitude sector (Otsuka et al., 2021). Since the solar cycle variations of magnetic and solar activities are correlated and magnetic activity has a significant influence on MSTID occurrence rates, evaluating the influence of solar activity proper asks to disentangle the influence of magnetic activity from that of solar activity. To this aim, we have plotted the MSTID occurrence rates separately for 3 categories corresponding to (a) low ( $A_m \leq 20$  nT), (b) moderate and high ( $A_m > 20$  nT) magnetic activity and (c) for all levels of magnetic activity. The annual occurrence rates of the Northern, Southern and low latitude EQ events have been plotted, from 2005 to 2010, in the corresponding Figures 8a–8c. Also plotted in Figure 8c are the “total” annual occurrence rates (Northern + Southern + EQ events) and the ratio of the Southern to Northern events. The annually averaged values of the solar flux index F10.7 are shown in a separate plot below Figure 8c.

For a given range of  $A_m$  values, the Northern annual occurrence rate is defined as the ratio between the number of night half-orbits for which a MSTID (MIN + MLN) was detected in the Northern hemisphere and the number of night half-orbits in the corresponding year in the same range of  $A_m$  values. The same definition holds for the Southern (MIS + MLS), EQ and the “total” annual occurrence rates. During the end of solar cycle 23, F10.7 decreases from 93 to 73 SFU from 2005 to 2007, then falls to very low values of 69.7 and 70.3 SFU in the 2008 and 2009 deep solar minimum, and rises again to 80 SFU in 2010 at the start of the new solar cycle 24. Figure 8 shows rather similar year to year variations of occurrence rates with no major influence of magnetic activity which, therefore, does not appear to induce any statistically significant bias in the observed variations of occurrence related to solar activity. The overall features observed in the 2005–2010 period may thus be considered as truly representative of the effect of solar activity proper. Three periods can be distinguished.

**2005–2007:** During the declining phase of solar cycle 23 with F10.7 decreasing from 92 to 73 SFU, the total occurrence rate increases from ~65% to 85% with some differences between the two hemispheres: in the North a regular increase (~20%–35%), nearly independent of magnetic activity, in the South an overall increase (~37%–53%) but only a minor variation at low magnetic activity with a 2006 maximum even slightly above the 2007 value. In equatorial regions a nearly constant level (~3–4%) with no obvious influence of solar activity. These results are in agreement with the above mentioned papers and with results of Park et al. (2010) based on CHAMP plasma data who showed an increase in the MSTID occurrence rates from ~15% to 17% in the 2000–2001 solar maximum to ~25%–27% at moderate solar activities in 2006–2007. Increased occurrence rates may arise from the shrinkage of the mid and low-latitude thermosphere and the lower plasma density in the F-region resulted from the steady decline of solar activity: these two parameters combine to decrease the integrated average ion-neutral collision frequency  $\langle \nu_{in} \rangle$  and amplify the maximum growth rate  $\gamma_{max}$  of the ionosphere instability helping the development of MSTIDs Perkins (1973)

$$\gamma_{max} \sim 3.10^{-4} \langle \nu_{in} \rangle^{-1} \cdot [\sin^2 D \cdot \sin^2(\theta/2) / \cos \theta] s^{-1}$$

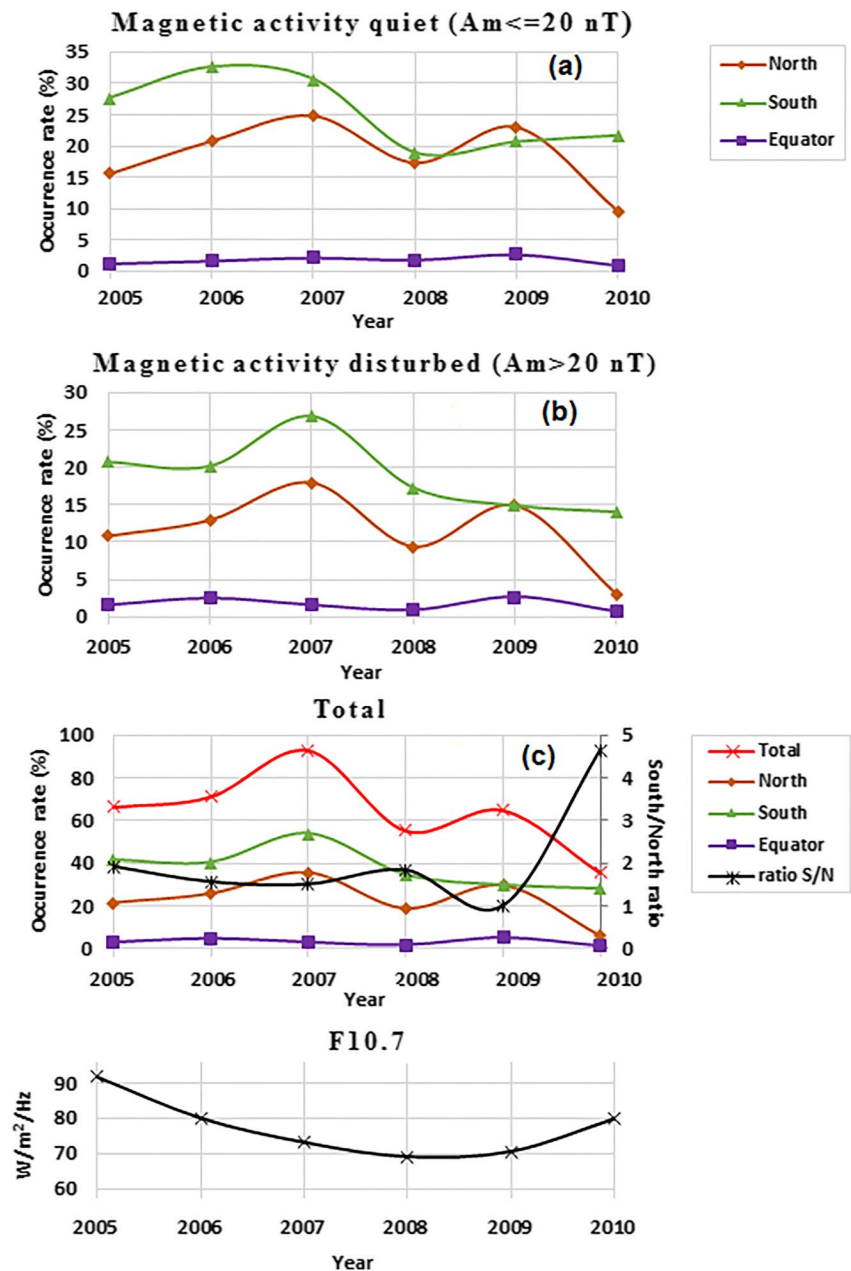


**Figure 8.** An overview of the Medium-Scale Traveling Ionospheric Disturbance (MSTID) occurrence variations as a function of solar activity, distinguishing two levels of magnetic activity, quiet ( $A_m < 20$ ) (a) and active ( $A_m > 20$ ) (b). The similarity between the two cases, allows to ascribe the year to year variations summarized in (c) (drawn for all levels of magnetic activity) to solar activity alone. The secondary maximum of occurrence of Northern MSTIDs in 2009 is associated with seasonal variation as shown in Section 6.

2008–2009: During the deep solar minimum with F10.7 values of 69.7 and 70.5, opposite variations are observed with first a sharp drop of occurrence rates in 2008 (–20% in the North and –28% in the South) followed by a rise in 2009 only in the North (~+30%) slightly above the Southern values maintained at their 2008 level. Interestingly, one may notice that two ground-based observations also reported similar variations: event rates measured over Brazil rise between 2005 and 2007 and drop sharply by ~25% in 2008 (Amorim et al. (2011), their Figure 5) and event rates in the Northern Central Pacific zone rise between 2006 and 2007 and fall by ~8% in 2008 (Duly et al. (2013), their Figure 3). In 2009 the average DEMETER occurrence rates rise by ~9% due to the increase of Northern MSTIDs alone since the Southern occurrence rates stay equivalent to their 2008 level. There are no

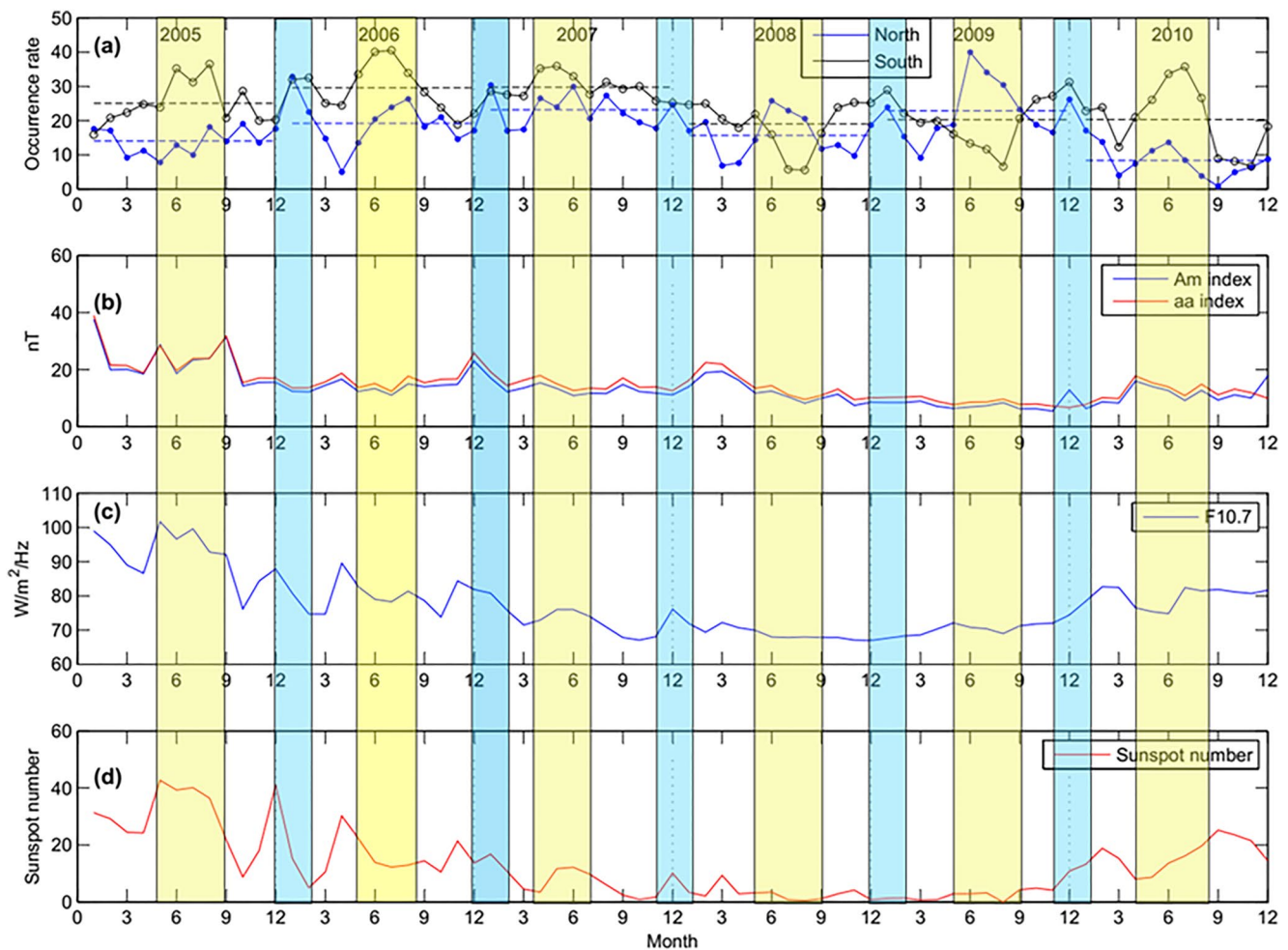


**Figure 9.** Monthly averages of Medium-scale traveling ionospheric disturbances occurrence rates from 2005 to 2010 with the corresponding averages of Am, F10.7 and SSN indices. Summer solstice months are highlighted in yellow for the Northern hemisphere, in blue for the Southern hemisphere.

2009 data in Amorim et al. (2011) but, according to Duly et al. (2013) the rise in the 2009 occurrence rate is  $\sim 10\text{--}15\%$ , thus similar to DEMETER. 2009 differs from 2008 by a very minor increase of solar activity of  $\sim 1.8$  SFU but a sizable drop of magnetic activity from  $aa = 14$  to  $aa = 8$  making 2009 the quietest year in the last century (Zerbo et al., 2012). Owing to the very low auroral activity and minor increase of solar activity, conditions in the thermosphere should not have varied significantly compared to those prevailing in 2008 as shown in Solomon et al. (2013) and, from Figure 6, only a very faint increase of the annual occurrence rate could only be expected. This is in agreement with the stability of the Southern occurrence rate but opposite to the sizable increase of the Northern occurrence rates.

**2010:** In the beginning of solar cycle 24, solar activity rises rapidly to a level comparable to the average level between 2005 and 2007. Southern occurrence rates get back to their average level prior to solar minimum but Northern occurrence rates drop to a low value of  $\sim 10\%$  in local summer (see Figure 9). A similar but much weaker trend was reported by Duly et al. (2013) from ground-based observations with a drop of 15% of occurrence rates between 2009 (67%) and 2010 (52%).

To summarize, while the general anti-correlation of MSTID occurrence with solar activity found by a number of early studies is confirmed between 2005 and 2007, a striking opposite evolution is observed at solar minimum with a sharp drop of the overall occurrence of MSTIDs in 2008 in spite of a very low F10.7 value, and a partial recovery in 2009 to a level yet lower than in 2007. In 2010, the occurrence of Southern events gets back to a level close to 2009 while Northern events drop to their smallest occurrence rate over the whole 6 year period.



The anomalous behavior during solar minimum already noticed in Figure 5 will be discussed in detail in the next section.

## 6. Solar Activity, Inter-Annual and Seasonal Variations of MSTID Occurrence

Statistical results displayed in Section 5 point to a more complex influence of solar activity on MSTID occurrence and their inter-hemispheric distribution than expected from previous studies, in particular during the deep solar minimum between solar cycles 23 and 24. In addition, satellite observations (Park et al., 2010), although obtained over periods of less variable solar activity, have shown that seasonal variations and geographic distribution of MSTIDs appear intricately coupled with the effects of solar activity. To proceed further in the analysis of the MSTID climatology, a combined analysis of inter-annual and seasonal variations of the Northern and Southern MSTID occurrence rates was performed and first illustrated in Figure 9 where have been plotted the monthly averages of the Northern and Southern occurrence rates and the corresponding monthly averages of the Am magnetic activity index, solar flux F10.7 and SSN solar activity index.

The upper plot clearly put in evidence seasonal peaks of occurrence around June and December summer solstices often with remarkable year to year differences in extent and amplitudes between the two hemispheres. To help visualize these features, we have highlighted respectively in light yellow and light blue the periods corresponding to these seasonal peaks of MSTID activity. The yellow ones, around the June solstice, extend generally from May to August thus shifted by ~1–2 months later than the solstice itself. The blue ones, around the December solstice, are shorter, generally extending from December to February, yet revealing the same tendency to be shifted later than the solstice. These consistent shifts suggest a “time constant” of the order of a month or two in evolution around solstices of the ionospheric and atmospheric parameters which control the development of MSTIDs.

A closer examination of Figure 9 helps to pinpoint several distinct features of the coupled inter-annual and seasonal variations. During the 2005–2007 declining phase of solar cycle 23, the worldwide MSTID activity is clearly dominated by Southern events with peaks of occurrence extending over several months around June solstices. Even if Northern occurrence rates also increase around June solstice, they stay at a lower level than the Southern ones, which accounts for the predominance of the annual average rate of Southern events. In 2005 and 2006, close to December solstices, shorter secondary maxima of occurrence are observed with similar amplitudes in both hemispheres. A noticeable evolution is observed in 2007 which looks as a transition year prior to the deep solar minimum of 2008–2009. The 2007 Southern peak of occurrence in June is slightly reduced but extends widely on both sides toward the neighbor December solstices while the Northern occurrence rates increase and, even if smaller than the Southern ones, display monthly variations rather similar to that of the Southern events. The deep solar minimum in 2008 and 2009 marks a striking evolution of the MSTID monthly variations: opposite to previous years, Southern occurrence rates strongly decrease between the March and September equinoxes and show a deep minimum around June solstice while the Northern occurrence rates maximize in the same period. Peaks of occurrence are still observed around the December solstice with rather similar amplitudes in both hemispheres. The very low Southern occurrence rates around June solstice together with the simultaneous high Northern peak of occurrence account for the overall predominance of Northern events in 2009. In 2010 with the initial rise of solar activity early in solar cycle 24, monthly variations of the Southern occurrence rates are back to those observed in 2005 and 2006 with a strong peak around June solstice. Even if showing a peak correlated with the Southern peak, the June solstice Northern occurrence rates stay at a much lower level than in 2005 and 2006.

Taking into account these results a detailed analysis of the MSTID geographic distribution at solstices and equinoxes was performed by sorting the observations among three periods:

- *Period 1* (2005, 2006, 2010) is characterized by a moderate solar activity ( $80 < F_{10.7} < 92.3$ ), marked seasonal variations of MSTID occurrence in both hemispheres and a significant predominance of Southern events with an average annual South/North event ratio of 1.6.
- *Period 2* (2007) a transition year prior to the deep solar minimum with a lower solar activity ( $F_{10.7} = 73.1$ ), high MSTID occurrence, smoother seasonal variations and a lower South/North event ratio of 1.3.
- *Period 3* (2008, 2009), the deep solar minimum with a very low solar activity ( $68.7 < F_{10.7} < 70.5$ ), characterized by a striking change in seasonal variations with the disappearance of the Southern peak of occurrence around June solstice and a resulting lower South/North event ratio of ~1.15 in 2008 and even ~0.9 in 2009, the only year when more MSTIDs were observed in the Northern hemisphere.



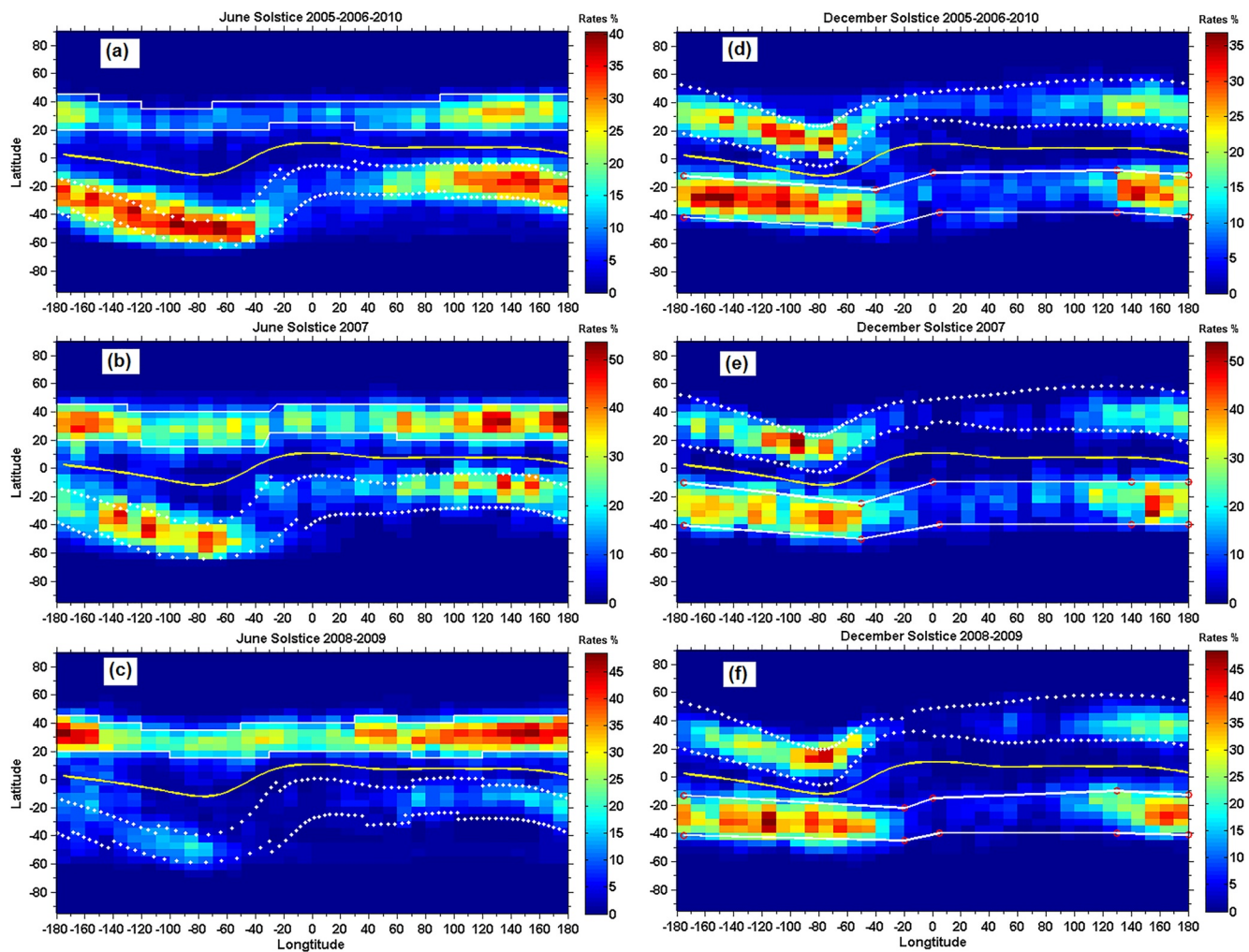


**Figure 10.** Seasonal geographical maps of Medium-scale traveling ionospheric disturbances (MSTID) occurrence rates at solstices shown separately for the 3 periods indicated in the text: [2005, 2006, 2010] with moderate solar activity, [2007] the transition year before the deep solar minimum and [2008, 2009] the deep solar minimum. The solid white lines indicate the boundaries of the MSTID areas of occurrence in the hemisphere where the Es layers are observed, North in June, South in December. The dotted white lines, in the opposite hemisphere, are the magnetic conjugates of these boundaries. The yellow line shows the position of the magnetic equator at the 650 km altitude of Detection of Electro-Magnetic Emissions Transmitted from Earthquake Regions.

Considering the extents and delays of the occurrence peaks with respect to the solstice and equinox revealed by Figure 9, the solstice and equinox “seasons” were defined as follows:

“June solstice”: months 5,6,7,8, “December solstice”: months 11,12,1,2

“March equinox”: months 2,3,4,5, “September equinox”: months 8,9,10,11

Presented in Figures 10 and 11 are the MSTID geographic distribution maps corresponding to the 4 solstice and equinox seasons with separate maps drawn for the 3 periods. These maps are organized by pixels  $10^\circ$  in longitude and  $5^\circ$  in latitude and in each pixel, the occurrence rate is defined as the ratio between the number of orbits with an event recorded in this pixel to the total number of orbits crossing this pixel during the interval of time corresponding to the map.

### 6.1. MSTID Occurrence Rates at June Solstices (Figures 10a–10c)

The first obvious feature, common to the 3 periods is the striking difference between the Northern and Southern MSTID areas: in the Northern hemisphere the MSTID areas are bounded by a set of line segments at constant geographic latitudes, close to  $\sim 20^\circ$  and  $\sim 40^\circ$ , indicated as white lines while Southern boundaries display large

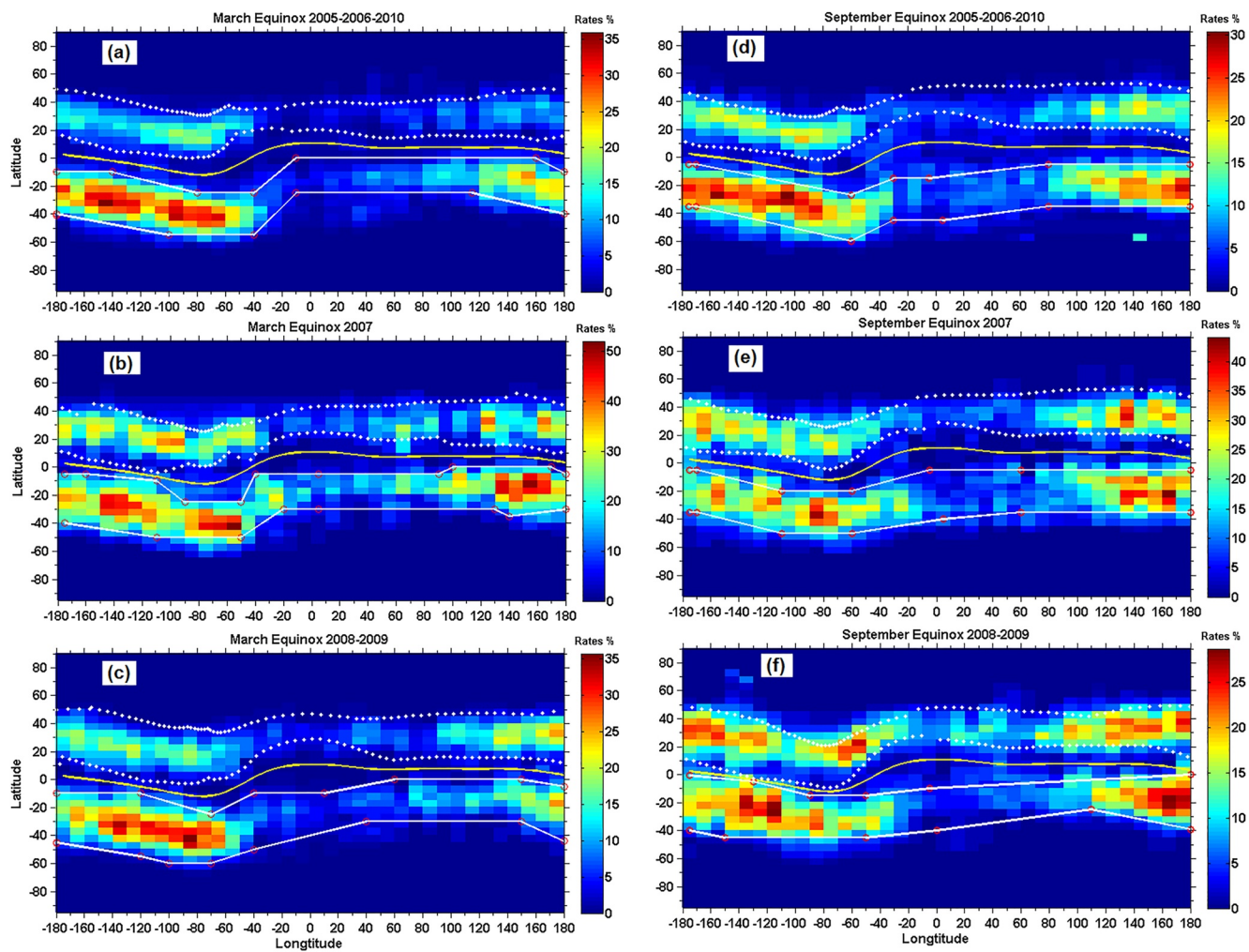


**Figure 11.** At Equinoxes, the less frequent Medium-scale traveling ionospheric disturbances are spread over the two hemispheres. The boundaries of the main areas of occurrence have been drawn as white solid lines in the Southern hemisphere where higher occurrence rates are observed. Their conjugates in the Northern hemisphere are shown as dotted white lines.

variations in geographic latitude as a function of longitude. Northern MSTIDs occur less frequently in 2005 and 2010 (see Figure 9) leading to the lower average occurrence rates in Period 1 (Figure 10a). The 2007 MSTID area extends to lower latitudes of  $\sim 15^\circ$  at longitudes  $[-120^\circ, -40^\circ]$ . The constant geographic latitudes of the Northern boundaries bear a remarkable similarity with the geographic distribution of Es layers averaged from December 2006 to January 2014 shown in Figure 5 of Yu et al. (2019). Following previous works by Wickert et al. (2004) and Wu et al. (2005), these authors have used the scintillations of the GPS signals received onboard the COSMIC satellite between December 2006 and January 2014 to detect the presence of Es layers at  $\sim 100$  km altitude along the propagation path of the GPS signal. A similar work was also performed by Arras et al. (2008). As shown by Figures 3 and 5d of Yu et al. (2019), Es layers develop at Northern mid latitudes during a 4–5 month period around June solstice within an area bounded by lines at nearly constant latitudes of  $\sim 24^\circ$  and  $50^\circ$  in the longitude sector  $[-15^\circ, 180^\circ]$ . In this longitude sector, the MSTID boundaries projected along the Earth's magnetic field lines to an altitude of 100 km, are located at latitudes  $28^\circ \pm 2^\circ$  and  $43^\circ \pm 2^\circ$  exactly in the center of the Es area. At longitudes less than  $-15^\circ$  the latitudes of the Es area boundaries decrease nearly linearly with longitudes by about  $10^\circ$  to reach  $\sim 14^\circ$  and  $\sim 40^\circ$  at  $\sim -70^\circ$  longitude. A similar quasi linear variation of the boundaries is observed between  $-180^\circ$  and  $-140^\circ$  longitudes. Es layers are significantly less frequent in the longitude sector  $[-70^\circ-140^\circ]$  as is the case in all 3 periods for Northern MSTIDs at June solstice that also maximize at latitudes lower by  $\sim 5^\circ$  than in other longitude sectors. The remarkable coincidence between the geographic distribution of MSTIDs and Es layers fully supports the “electrified MSTID” model proposed by Tsunoda and Cosgrove (2001)

and Tsunoda (2006). In this model, the structured electric fields associated with the Es layers at  $\sim 100$  km altitude couple along Earth's magnetic field lines to the plasma in the F-region at 250 km altitude and play a key role to enhance the growth rate of the ionospheric instability and allow large amplitude MSTIDs to develop. This process accounts for the high occurrence and amplitudes of the observed MSTIDs. Based on outcomes of the SD-WACCM general circulation model, Yu et al. (2019) have also put in evidence a close correlation between the geographic distribution of Es layers and the areas where the divergence of the ion velocity along magnetic field lines maximize during Northern summer in the altitude range 97–114 km. This area is located between constant latitudes of  $\sim 30^\circ$  and  $\sim 60^\circ$  in the Northern hemisphere, thus connected to the MSTID area. Even if they maximize in the collisional lower ionosphere, these disturbances extends to higher altitudes. Considering their close coincidence with the MSTID area and their impact on the dynamics of the upper ionosphere, they may also play a role in the MSTID development that should be considered by theoretical and numerical models.

The Southern magnetic conjugates of the Northern boundaries have been shown by white dots and superpose nearly perfectly with the observed boundaries of the Southern MSTID area in Periods 1 and 2 (Figures 10a and 10b) bringing a remarkable observational validation of the Yokoyama (2014) model of inter-hemispheric conjugacy of electrified MSTIDs. During Northern summer, no Southern Es layers are observed (Arras et al., 2008; Yu et al., 2019) and the mapping of Northern electric fields to the Southern conjugate regions only provide the proper conditions for the development of local electrified MSTIDs. During the deep solar minimum of 2008–2009 (Period 3, Figure 10c), the occurrence rates of Southern MSTIDs fall to very low values and concentrate over a reduced zone around the center of the conjugate area of the Northern MSTIDs. This region corresponds to the maximum occurrence of the Northern Es layers again showing the key role played by structured electric fields mapped from the Es area to its conjugate. On the other hand, Figures 10a and 10b shows that the highest occurrence rate areas in opposite hemispheres are not always magnetically conjugated. As an example, in 2007, the occurrence in the North at longitudes  $[-180^\circ, -140^\circ]$  is larger than in the conjugate Southern sector while a reverse situation occurs with high occurrence in the South at longitudes  $[-140^\circ, -60^\circ]$  and significantly less events observed over Northern conjugated longitudes. Differences between the upper atmosphere and ionosphere over conjugated longitude sectors likely result in differences in the growth rates of MSTIDs and their dynamics. An obvious difference arises from the opposite seasonal variations imposed on conjugated upper atmosphere and ionosphere. Additional and likely more important differences arise from the differences between the geographic latitudes of conjugate areas. As an example at longitudes  $[-140^\circ, -60^\circ]$  Southern MSTIDs occur at geographic latitudes significantly higher (by  $\sim 10^\circ$ – $15^\circ$ ) than the conjugates Northern latitudes. Finally, AGW, which have been advocated as an efficient seeding process of MSTIDs, may occur much more frequently in some longitude sectors of a given hemisphere, thus possibly increasing the local MSTID occurrence rates.

Obvious in Figures 9 and 10c, the major feature of the MSTID climatology is the nearly disappearance of Southern events around June solstice during the 2008–2009 deep solar minimum (Period 3) while Northern large summer peaks of occurrence are still observed, even amplified in 2009 with respect to the 2007 and 2008 values. Monthly Southern occurrence rates fall to extremely low values of  $\sim 5\%$  in July and August 2008 and  $\sim 10\%$  in August 2009. Averaged over 4 months around June solstice (May–August), the South/North event ratio falls abruptly from  $\sim 1.35$  in 2007 to  $\sim 0.5$  in 2008 and  $\sim 0.4$  in 2009, the only year in the 2005–2010 period with an annually averaged occurrence rate lower in the South than in the North. The Northern Es time series in Figure 3 of Yu et al. (2019) do show in 2008 and 2009 the usual 4–5 month period of occurrence with similar characteristics as in other years and no variation linked to solar activity. In 2009 the observed slight enhancements of the S4max index denote an increased number and/or larger amplitudes of Es layers and which may account for the higher occurrence of Northern MSTIDs, up to 40%, the largest level among the 6 years of the DEMETER database, with most events detected over South-East Asia, China and Japan and moderate occurrence rates extending toward Eastern Europe.

The drastic drop of Southern MSTIDs around June solstice in 2008–2009 should result from substantial modifications of the processes involved in their generation and development, in particular (a) the mapping of the Northern Es electric fields to the conjugate Southern hemisphere and (b) the effectiveness of the ionospheric instability that controls the growth of MSTIDs in the Southern hemisphere.

The inter-hemispheric mapping of electric fields depends on two main factors. The first one is the spatial structure and orientation of the Northern Es electric fields: it is known (e.g., Park, 1979) that electric fields with shorter spatial scale lengths maps less efficiently to the conjugate region. A preliminary investigation of the



DEMETER data did not show major changes of the spatial wavelengths of MSTIDs in 2008–2009 but a more thorough analysis of the whole set of measurements available from DEMETER is needed and will be presented in a subsequent report. The second factor is the dependence of the mapping process upon ionospheric conductivity profiles at both ends of the magnetic field lines. The well documented seasonal inter-hemispheric differences in the ionosphere mainly arise from the differences between the dominant photochemical production and loss processes and between thermospheric winds. They may be amplified during the deep solar minimum, especially during the Southern winter hemisphere with larger differences in the conductivity profiles thus on the mapping of electric fields. A less efficient electric field mapping would result in a similar decline of the Southern MSTID occurrence. A more detailed modeling of the seasonal variations of the conjugate mapping of electric fields is needed to ascertain its possible impact on the seasonal inter-hemispheric differences of MSTID occurrence.

The actual growth rate of the ionospheric instability also plays a major role in the rise and development of MSTIDs, thus on the occurrence of Southern MSTIDs. It depends on the altitude profiles of the local ionospheric conductivities directly related to the characteristics of the neutral atmosphere and ionosphere. The electrified MSTID model, complemented by the inter-hemispheric mapping of electric fields, works well for standard conditions of the upper atmosphere and ionosphere, as shown by Yokoyama (2014). However, it may lose efficiency for notably different conditions such as those met in the Southern winter ionosphere during the 2008–2009 deep solar minimum. Modeling efforts are thus needed to quantitatively ascertain the impact of the substantial solar minimum shrinkage of both the upper neutral atmosphere and ionosphere reported by Araujo-Pradere et al. (2011), Nanan et al. (2012), Balan et al. (2013) and Solomon et al. (2013). In addition to the plasma density and composition in the lower ionosphere, thermospheric winds and wind shears that control in part the occurrence and propagation of AGW have also a noteworthy effect on the triggering of MSTIDs and their dynamics, in particular for conjugate events (Narayanan et al., 2018). The sizable evolution of thermospheric winds at low solar activity (e.g., Drob et al., 2015) may impact the MSTID growth rates and lower them in the Southern region conjugate to the area of Northern events. This would lead to the weakening and even disappearance of Southern MSTIDs. Global modeling studies are indeed needed to help in a better understanding of the effect of seasonal variations on the MSTID hemispheric asymmetry. Before ending this section, one may also mention that worldwide, cyclical meteorological phenomena have a sizable impact on the lower atmosphere by modifying the wind regime and orographic gravity wave activity. These events vary in intensity from year to year as with a similar variable impact on the lower atmosphere and on the forcing of the ionosphere from below which is thought to be a likely mechanism to trigger MSTIDs. Thus year to year variations in the occurrence of MSTIDs may, in part, reflect the year to year variations of meteorological conditions.

## 6.2. MSTID Occurrence Rates at December Solstices (Figures 10d–10f)

At December solstices, MSTIDs occur less frequently and their geographic distribution displays both similarities and differences with the distribution observed at June solstice. As Northern MSTIDs in June, Southern MSTIDs in December are detected in an area with boundaries organized along geographic coordinates: as shown in Figures 10d–10f the latitudes of the boundaries decrease slowly and nearly linearly with longitude in the longitude sector  $[-180^\circ, -40^\circ]$  with an opposite variation in the longitude sector  $[-40^\circ, 20^\circ]$ . On the contrary the boundaries of the MSTID area in the opposite hemisphere are characterized by highly varying latitudes as a function of longitude. The underlying physical processes are similar to those already discussed for June solstice: around December solstice satellite observations point out the existence of Es layers at  $\sim 100$  km altitude over Southern mid-latitudes and local electrified MSTIDs develop from the coupling between the slightly unstable plasma in the F region and the structured electric fields associated with these Es layers. In December, Southern Es occur during a shorter period ( $\sim 2$ – $3$  months) than the Northern Es in June and the values of the S4max index, lower than those in June in the North (see Figure 2 of Yu et al., 2019), are indicative of fewer and/or less intense Es layers in accordance with the overall lower occurrence of Southern MSTIDs around December solstice. The Es area boundaries taken from Figure 6b of Yu et al. (2019), are close and parallel to the Southern MSTID area boundaries. Alike Northern MSTIDs at June solstice, Southern MSTIDs at December solstice develop along magnetic field lines issued from the Es area. The Northern conjugates of the MSTID Southern boundaries, shown as white dots on Figures 10d–10f closely correspond to the boundaries of the observed Northern MSTID area, reproducing an inter-hemispheric pattern of MSTID distribution symmetrical to what happens at June solstice, again in full agreement with the conjugate electrified MSTID model of Yokoyama (2014).

A few noticeable features can be observed in Figures 10d–10f. In all 3 periods, Southern MSTIDs maximize at longitudes from  $\sim 110^\circ$  to  $180^\circ$  and  $-180^\circ$  to  $-50^\circ$  but are very scarce between  $\sim -30^\circ$  and  $\sim 120^\circ$  longitudes. The conjugate events in the North display a similar longitudinal distribution with a maximum of occurrence in the longitude sector  $[-130^\circ, -60^\circ]$  where the MSTID area is located at the lowest geographic latitudes of  $\sim 10^\circ$ – $\sim 20^\circ$ . Specific favorable conditions in the neutral upper atmosphere and ionosphere for the instability to develop may be encountered at such low geographic latitudes in the winter Northern hemisphere. A major difference between the June and December solstices lies in the year to year evolution of the South/North event ratio which will be discussed at the end of Section 6.

### 6.3. MSTID Occurrence Rates at Equinoxes: March (Figures 11a–11c) and September (Figures 11d–11f)

As shown by statistical results from Yu et al. (2019) and Li et al. (2020) the occurrence and geographic distribution of Es layers around equinoxes looks like a fuzzy transition between the very clear maxima of occurrence at solstices in opposite hemispheres. Es layers are significantly less frequent, with occurrence rates between 30% and 40% of those at solstices and, as an average picture, in March they migrate from Southern to Northern mid latitudes maximizing, on the average, at low latitudes of  $10^\circ$ – $20^\circ$  while a symmetric migration, from Northern to Southern mid latitudes, happens in September. These features explain quite well the lower occurrence rates of MSTIDs at both equinoxes, about  $\sim 50\%$ – $\sim 25\%$  compared to those at solstices. As seen in Figures 11a–11c around March, Southern MSTIDs clearly predominate over Northern events in all three periods, thus independently of solar activity. A similar dissymmetry is observed in Figure 11d around September for years with a moderate solar activity (period 1), less marked in 2007 (Figure 11e) and nearly vanishing during the deep solar minimum of 2008–2009 (Figure 11f). As at solstices, MSTIDs maximize from  $\sim 100^\circ$  to  $\sim -40^\circ$  longitudes from Australia to South America in the Southern hemisphere and from Eastern Asia to Northern America in the North with weak local Northern and Southern maxima occurring along conjugated longitude sectors. The Southern MSTID boundaries (thick white lines) have been mapped to their Northern magnetic conjugates (white dotted contours), showing that MSTIDs do occur within conjugate areas in opposite hemispheres again in full agreement with the Yokoyama model of conjugated electrified MSTIDs.

Two detailed features of interest may be noticed. In March 2007, the unusual increase of Southern MSTIDs is associated with a similar uncommon extent of the local summer Es layers till March in the Es maps of Yu et al. (2019), providing additional support to the prominent role of Es layers in the development of MSTIDs. In September 2008–2009, at longitudes from  $-140^\circ$  to  $-50^\circ$ , Southern MSTIDs extend to very low magnetic latitudes slightly less than  $5^\circ$ , indicating that favorable ionospheric conditions are encountered even close to magnetic equator. On the contrary, the corresponding Northern MSTIDs only occur at magnetic latitude above  $\sim 15^\circ$  reflecting a significant asymmetry between the Northern and Southern ionospheres in this longitude sector during very low solar activity.

### 6.4. Inter-Hemispheric Differences and Their Seasonal and Solar Activity Dependence

The Northern and Southern MSTID occurrence rates display a complex interplay of solar activity and seasonal variations. To disentangle these two effects, we have drawn in Figure 12, separately for the solstices and equinoxes, the annual variations of the Northern and Southern MSTID occurrence rates and the South/North ratio in the period 2005–2010. As already shown in Figure 8, the F10.7 solar flux index decreases from  $\sim 90$  to  $\sim 70$  between 2005 and the deep solar minimum in 2008–2009 and rises again in 2010 to the same value of  $\sim 80$  as in 2006.

Southern MSTIDs are more frequent than Northern MSTIDs in all seasons except at June solstices during the deep solar minimum of 2008–2009 but the annual variations of the seasonally averaged occurrence rates display distinct features for each season.

At June solstices, Northern occurrence rates show a rather regular increase from 2005 to 2009 before a sharp drop in 2010, while the high Southern rates of  $\sim 35\%$  between 2005 and 2007 with a moderate maximum in 2006, fall drastically at solar minimum to increase again in 2010 to the same value as in 2007. The strongly opposite variations of Northern and Southern MSTIDs in 2008 and 2009 might be interpreted as a consequence of large inter-hemispheric differences in the thermosphere and ionosphere during the deep solar minimum. MSTID activity would be favored in the Northern summer hemisphere but impeded in the Southern winter hemisphere. As



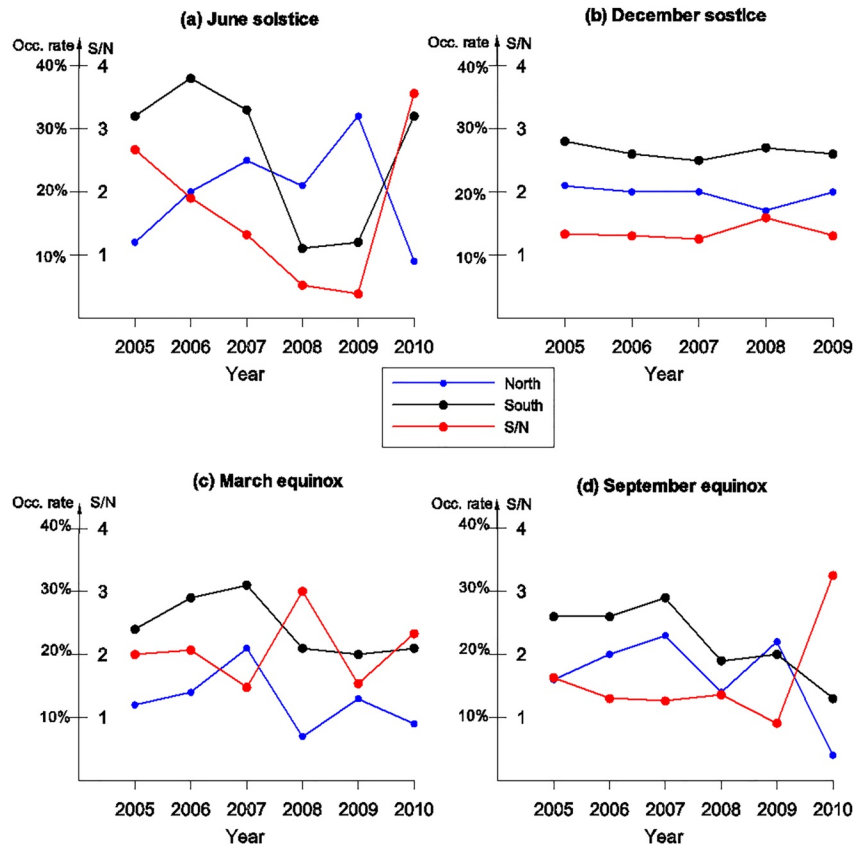


**Figure 12.** Northern (black) and Southern (blue) average occurrence rates and the ratio of Southern to Northern occurrence (red) rates from 2005 to 2010 shown separately in panels (a and b) for the June and December solstices, and in panels (c and d) for the March and September equinoxes.

already mentioned, both a less efficient mapping of Northern electric fields to the Southern hemisphere and/or a lower growth rate of the ionospheric instability in the winter ionosphere may lead to such a situation. However, the South/North ratio (S/N) decreases regularly between 2005 and 2009, from  $\sim 2.7$  in 2005 to  $\sim 0.5$  and  $\sim 0.4$  in 2008 and 2009. This remarkably regular trend over 5 years seems more consistent with a long term effect of the declining solar activity on the inter-hemispheric differences of MSTID activity. In 2010, the solar activity is back to its 2006–2007 level as well as the Southern MSTID occurrence rates. One would thus expect that Northern occurrence rates would stay close to their  $\sim 23\%$  2006–2007 level while they fall to a surprisingly low value of  $\sim 8\%$ , leading to a large S/N value of  $\sim 3.4$ . At June solstice, the development of Southern MSTIDs rely on the existence of local electric fields mapped from those associated with Northern Es layers: the similarity of Southern occurrence rates with those in 2006 suggests that the 2010 “electric field” conditions are similar as in 2006. The abnormally low Northern occurrence rates might therefore be linked to a significant modification of the conditions in the Northern ionosphere that control the generation and development of the local MSTIDs. As mentioned in Section 6.1, unusual meteorological conditions and their consequences on the forcing of the ionosphere from below may play a significant role in such anomalous effects.

Contrary to June solstices, December solstices are characterized by practically constant Northern and Southern occurrence rates of respectively  $\sim 20\%$  and  $27\%$  between 2005 and 2009. Due to the end of DEMETER operation early in December 2010, it was not possible to determine the exact value of the 2010 occurrence rates. However, from the November and early December data, it was concluded that the occurrence rates for the 2010 December solstice should also stay similar to those in the previous 5 years. Thus, opposite to what happens at June solstices, solar activity does not play a significant role in the worldwide MSTID activity during December solstices and, in addition, the absence of any “anomalous” year to year variation must be noticed. Further studies, based, in particular, on improved numerical models including the actual ionospheric seasonal variations, are needed to understand the surprising opposite behavior of MSTID activity at June and December solstices.

At both equinoxes, Northern and Southern occurrence rates are significantly higher and regularly increasing between 2005 and 2007, then decrease to nearly constant levels during the last 3 years, 2008 to 2010 with two exceptions: Northern occurrence rates show a relative maximum in 2009, with a predominant peak at September equinoxes followed by a drastic fall to  $\sim 5\%$  in 2010 with a simultaneous decline of the Southern occurrence rates. At September equinoxes, the peak in 2009 and the moderate but regular decline of the South/North ratio between 2005 and 2009 are reminiscent of similar effects observed at June solstices. This likely arises from the 4 months averaging to compute the seasonal occurrence rates: month 8 (August) is taken into account both in the “June solstice” and “September equinox” periods and, as shown in Figure 9, the increase of the 2009 Northern occurrence rates around June solstice extends over 4 months from June to September. At March equinoxes the South/North ratio does not show any definite trend associated to solar activity, with only a local increase in 2008.

## 7. Summary and Conclusions

Using thermal ion measurements from the DEMETER satellite, we have performed a statistical study of the mid-latitude night-time Medium Scale Traveling Ionospheric Disturbances (MSTIDs) detected from the quasi-periodic undulations of the  $O^+$  ion density  $N(O^+)$ . The 6 years of satellite operation, from 2005 to 2010, encompass the end of solar cycle 23, from 2005 to 2007, with a moderate, decreasing solar activity, the deep solar minimum in 2008–2009 and the rise of activity in 2010 at onset of solar cycle 24. The nearly continuous operation of the satellite at magnetic latitudes less than  $60^\circ$  and at an almost constant  $22 \pm 0.5$  local time allowed an in depth study of the MSTID geographic distribution, their response to the varying magnetic and solar activities and their seasonal variations. The main outcomes of this study may be summarized as follows:

1. Over the whole 6 year period 2005–2010, MSTIDs are detected very frequently on almost 30%–40% of the orbits under the form of quasi-periodic  $N(O^+)$  oscillations corresponding to average wavelengths of  $\sim 300$ – $400$  km in good agreement with those deduced from ground-based optical or TEC measurements.
2. Mid-latitude MSTIDs, with part of them extending to magnetic latitudes lower than  $\sim 15^\circ$ , are by far the major population, hence the main subject of our statistical study. Equatorial events observed within  $\leq 10^\circ$  of the magnetic equator are a minor, yet interesting, population that will be the subject of a forthcoming study. The annually averaged geographic distribution shows areas of highest occurrence rates in the Southern hemisphere from Australia to South America with a lower maximum in the Northern hemisphere over South-East Asia and the Eastern Pacific. Global occurrence rates maximize at low magnetic activity and decrease regularly by a factor  $\sim 3$  during disturbed periods. Averaged over the 6 year period, night-time MSTIDs occur  $\sim 1.7$  times more frequently in the Southern than in the Northern hemisphere.
3. The worldwide total occurrence rates increase as solar activity decreases, to reach a maximum events probability of 50%–60% per orbit in 2007 but decreases markedly during the 2008–2009 deep solar minimum contrary to the expected trend predicted by previous studies. This unexpected variation arises from the nearly disappearance of Southern MSTIDs around June solstice indicating either a less efficient mapping of electric fields from the Northern  $E_s$  layers to the Southern ionosphere and/or a strong decrease of the growth rate in the wintertime ionosphere at low solar activity. At June solstice, the South/North event ratio decreases regularly from 2.7 in 2005 to 0.4 in 2009 at the end of the deep solar minimum the only year when MSTIDs are more frequent in the Northern than in the Southern hemisphere.
4. The seasonal maps of MSTID occurrence display a remarkable difference between solstices and equinoxes. At solstices, in the summer hemisphere, MSTIDs maximizes over a band parallel to the geographic equator in the North or slightly inclined with respect to the equator in the South. These areas of occurrence fit nicely with those of  $E_s$  layers derived from the analysis of scintillations on the GPS signals received on-board CHAMP and COSMIC satellites as shown by Lee et al. (2021). In the winter hemisphere, in absence of local  $E_s$  layers, MSTIDs are still frequently observed in the magnetically conjugated area of the summer hemisphere events. These results provide a new and strong observational support to the key role played by the structured electric fields associated with  $E_s$  layers in the initiation and development of electrified MSTIDs and to their inter-hemispheric model of development based on the mapping of  $E_s$  electric fields to the conjugate hemisphere.

At equinoxes, MSTIDs are significantly less frequent than at solstices with a general predominance of Southern events except around September during the deep solar minimum. They maximize between Australia and South America and, to a lesser extent, over South-East Asia and the Northern Pacific. The geographic

distribution indicates that MSTIDs develop over conjugate areas in opposite hemispheres, again showing that the inter-hemispheric coupling of Es electric fields play a major role in their development.

5. The analysis of the Southern and Northern occurrence rates variations with solar activity have shown a striking and unexpected seasonal effect. At June solstice, the South/North event ratio displays a marked and continuous decline between 2005 and 2009 correlated with the decrease of solar activity, dropping from  $\sim 2.7$  in 2005 to  $\sim 0.4$  in 2009 at the end of the deep solar minimum and the only year with more Northern than Southern events. On the contrary, at December solstice, the South/North event ratio stays practically constant at  $\sim 1.2$  over the same period 2005 to 2009. Since DEMETER observations provide a definite evidence of the occurrence of “electrified” MSTIDs associated with the underlying Es layers, the nearly disappearance of Southern MSTIDs at June solstice must result from substantial modifications in the upper atmosphere and ionosphere, likely more sensitive in the winter Southern hemisphere, that would lead to a less efficient electric field mapping and/or to a lower MSTID growth rate. On the contrary, at December solstice, the South/North event ratio stays constant irrespective of the level of solar activity, indicating that no such variation of the inter-hemispheric asymmetry linked to solar activity would occur in this season. These new results call for an extensive effort in numerical modeling to decipher the physical processes in the upper atmosphere and ionosphere associated with solar activity and seasonal variations which impact the MSTID generation and development.

### Data Availability Statement

The SSN and F10.7 solar indices and the am magnetic activity index were provided by the following web sites: <http://solarscience.msfc.nasa.gov/SunspotCycle.shtml> and <https://www.swpc.noaa.gov/phenomena/f107-cm-radio-emissions>. DEMETER data are accessible from <https://cdpp-archive.cnes.fr>. Am and aa indices can be found at ISGI—International Service of Geomagnetic Indices (<http://isgi.unistra.fr>).

### Acknowledgments

The DEMETER satellite was built and operated by CNES teams from the Toulouse Space Center. The work of C.T. Nguyen was supported by the Vietnam Academy of Science and Technology (project VAST05.04/20-21). The authors wish to thank the referees for helpful and constructive remarks.

### References

- Amorim, D. C. M., Pimenta, A. A., Bittencourt, J. A., & Fagundes, P. R. (2011). Long-term study of medium-scale traveling ionospheric disturbances using OI 630 nm all-sky imaging and ionosonde over Brazilian low latitudes. *Journal of Geophysical Research*, *116*(A6), A06312. <https://doi.org/10.1029/2010JA016090>
- Araujo-Pradere, E. A., Redmon, R., Fedrizzi, M., Viereck, R., & Fuller-Rotwell, T. J. (2011). Some characteristics of the ionosphere behavior during the solar cycle 23-24 minimum. *Solar Physics*, *274*, 439–456. <https://doi.org/10.1007/s11207-011-9728-3>
- Arras, C., Wickert, J., Beyerle, G., Heise, S., Schmidt, T., & Jacobi, C. (2008). A global climatology of ionospheric irregularities derived from GPS radio occultation. *Geophysical Research Letters*, *35*(14), L14809. <https://doi.org/10.1029/2008GL034158>
- Balan, N., Rajesh, P. K., Sripathi, S., Tulasiram, S., Liu, J. Y., & Bailey, G. J. (2013). Modeling and observations of the North-South ionospheric asymmetry at long deep solar minimum. *Advances in Space Research*, *52*(3), 375–382. <https://doi.org/10.1016/j.asr.2013.04.003>
- Beach, T. L., Kelley, M. C., Kintner, P. M., & Miller, C. A. (1997). Total electron content variations due to non-classical traveling ionospheric disturbances: Theory and Global Positioning System observations. *Journal of Geophysical Research*, *102*(A4), 7279–7292. <https://doi.org/10.1029/96JA02542>
- Behnke, R. A. (1979). F-layer height bands in the nocturnal ionosphere over Arecibo. *Journal of Geophysical Research*, *84*(A3), 974–978. <https://doi.org/10.1029/ja084ia03p00974>
- Berthelier, J. J., Godefroy, M., Leblanc, F., Seran, E., Peschard, D., Gilbert, P., & Artru, J. (2006). IAP, the thermal plasma analyzer on DEMETER. *Planetary and Space Science*, *54*(5), 487–501. <https://doi.org/10.1016/j.pss.2005.10.018>
- Brigham, E. O. (1974). *The fast fourier transform*. Prentice-Hall Inc. 252.
- Burke, W. J., Martinis, C. R., Lai, P. C., Gentile, L. C., Sullivan, C., & Pfaff, R. F. (2016). C/NOFS observations of electromagnetic coupling between magnetically conjugate MSTID structures. *Journal of Geophysical Research: Space Physics*, *121*(3), 2569–2582. <https://doi.org/10.1002/2015JA021965>
- Candido, C. M. N., Pimenta, A. A., Bittencourt, J. A., & Becker-Guedes, F. (2008). Statistical analysis of the occurrence of medium-scale traveling ionospheric disturbances over Brazilian low latitudes using OI 630.0 nm emission all-sky images. *Geophysical Research Letters*, *35*(17), L17105. <https://doi.org/10.1029/2008GL035043>
- Cosgrove, R. B., & Tsunoda, R. T. (2004). Instability of the E-F coupled nighttime mid-latitude ionosphere. *Journal of Geophysical Research*, *109*(A4), A04305. <https://doi.org/10.1029/2003JA010243>
- Ding, F., Wan, W., Xu, G., Yu, T., Yang, G., & Wang, J. (2011). Climatology of medium-scale traveling ionospheric disturbances observed by a GPS network in central China. *Journal of Geophysical Research*, *116*(A9), A09237. <https://doi.org/10.1029/2011JA016545>
- Drob, D. P., Emmert, J. T., Meriwether, J. W., Makela, J. J., Doornbos, E., Conde, M., et al. (2015). An update to the Horizontal Wind Model (HWM): The quiet time thermosphere. *Earth and Space Science*, *2*(7), 301–319. <https://doi.org/10.1002/2014EA000089>
- Du Castel, F., & Faynot, J.-M. (1964). Some irregularities observed simultaneously in the upper and lower ionosphere at middle latitudes. *Nature*, *204*(4962), 984–985. <https://doi.org/10.1038/204984a0>
- Duly, T. M., Chapagain, N. P., & Makela, J. J. (2013). Climatology of nighttime MSTIDs in the central Pacific and South America sectors. *Annales Geophysicae*, *31*(12), 2229–2237. <https://doi.org/10.5194/angeo-31-2229-2013>
- Fathy, I., Amory-Mazaudier, C., Fathy, A., Mahrous, A. M., Yumoto, K., & Ghamry, E. (2014). Ionospheric disturbance dynamo associated to a coronal hole: Case study of 5–10 April 2010. *Journal of Geophysical Research: Space Physics*, *119*(5), 4120–4133. <https://doi.org/10.1029/2013JA019510>

- Figueiredo, C. A. O. B., Takahashi, H., Wrasse, C. M., Otsuka, Y., Shiokawa, K., & Barros, D. (2018). Investigation of nighttime MSTIDs observed by optical thermosphere imagers at low latitudes: Morphology, propagation direction, and wind filtering. *Journal of Geophysical Research: Space Physics*, *123*(9), 7843–7857. <https://doi.org/10.1029/2018JA025438>
- Frissell, N. A., Baker, J. B. H., Ruohoniemi, J. M., Gerrard, A. J., Miller, E. S., Marini, J. P., et al. (2014). Climatology of medium-scale traveling ionospheric disturbances observed by the midlatitude Blackstone SuperDARN radar. *Journal of Geophysical Research: Space Physics*, *119*(9), 7679–7697. <https://doi.org/10.1002/2014JA019870>
- Garcia, F. J., Kelley, M. C., Makela, J. J., Sultane, P. J., Pi, X., & Musman, S. (2000). Mesoscale structure of the midlatitude ionosphere during high geomagnetic activity: Airglow and GPS observations. *Journal of Geophysical Research*, *105*, 18417–18427. <https://doi.org/10.1029/1999JA000306>
- Grocott, A. K., Hosokawa, K., Ishida, T., Lester, M., Milan, S. E., Freeman, M. P., et al. (2013). Characteristics of medium-scale traveling ionospheric disturbances observed near the Antarctic Peninsula by HF radar. *Journal of Geophysical Research: Space Physics*, *118*(9), 5830–5841. <https://doi.org/10.1002/jgra.50515>
- Helmholtz, J. F., & Intema, H. T. (2012). Very large array observations of disturbed ion flow from the plasmasphere to the nighttime ionosphere. *Radio Science*, *47*(6), RS0K03. <https://doi.org/10.1029/2012RS004979>
- Hoffmann, L., Xue, X., & Alexander, M. J. (2013). A global view of stratospheric gravity wave hotspots located with Atmospheric Infrared Sounder observations. *Journal of Geophysical Research: Atmospheres*, *118*(2), 416–434. <https://doi.org/10.1029/2012JD018658>
- Huang, F., Dou, X., Lei, J., Lin, J., Ding, F., & Zhong, J. (2016). Statistical analysis of nighttime medium-scale traveling ionospheric disturbances using airglow images and GPS observations over central China. *Journal of Geophysical Research: Space Physics*, *121*(9), 8887–8899. <https://doi.org/10.1002/2016JA022760>
- Husin, A., Abdullah, M., & Momani, M. A. (2011). Observation of medium-scale traveling ionospheric disturbances over Peninsular Malaysia based on IPP trajectories. *Radio Science*, *46*(2), RS2018. <https://doi.org/10.1029/2010RS004408>
- Ishida, T., Hosokawa, K., Shibata, T., Suzuki, S., Nishitani, N., & Ogawa, T. (2008). SuperDARN observations of daytime MSTIDs in the auroral and mid-latitudes: Possibility of long-distance propagation. *Geophysical Research Letters*, *35*(13), L13102. <https://doi.org/10.1029/2008GL034623>
- Jacobson, A. R., Carlos, R. C., Massey, R. S., & Wu, G. (1995). Observations of traveling ionospheric disturbances with a satellite-beacon radio interferometer: Seasonal and local time behavior. *Journal of Geophysical Research*, *100*(A2), 1653–1665. <https://doi.org/10.1029/94JA02663>
- Kelley, M. C., & Fukao, S. (1991). Turbulent upwelling of the mid-latitude ionosphere, 2: Theoretical framework. *Journal of Geophysical Research*, *96*(A3), 3747–3753. <https://doi.org/10.1029/90ja02252>
- Kelley, M. C., & Makela, J. A. (2001). Resolution of the discrepancy between experiment and theory of mid-latitude F-region structures. *Geophysical Research Letters*, *28*(13), 2589–2592. <https://doi.org/10.1029/2000gl012777>
- Kelley, M. C., Makela, J. J., Saito, A., Aponte, N., Sulzer, M., & Gonzalez, S. A. (2000). On the electrical structure of airglow depletion/height layer bands over Arecibo. *Geophysical Research Letters*, *27*(18), 2837–2840. <https://doi.org/10.1029/2000gl000024>
- Kil, H., & Paxton, L. J. (2017). Global distribution of nighttime medium-scale traveling ionospheric disturbances seen by Swarm satellites. *Geophysical Research Letters*, *44*(18), 9176–9182. <https://doi.org/10.1002/2017gl074750>
- Kotake, N., Otsuka, Y., Ogawa, T., Tsugawa, T., & Saito, A. (2007). Statistical study of medium-scale traveling ionospheric disturbances observed with the GPS networks in southern California. *Earth Planets and Space*, *59*(2), 95–102. <https://doi.org/10.1186/bf03352681>
- Kotake, N., Otsuka, Y., Tsugawa, T., Ogawa, T., & Saito, A. (2006). Climatological study of GPS total electron content variations caused by medium-scale traveling ionospheric disturbances. *Journal of Geophysical Research*, *111*(A4), A04306. <https://doi.org/10.1029/2005JA011418>
- Lebreton, J. P., Sverak, S., Travnicek, P., Maksimovic, M., Klinge, D., Merikallio, S., et al. (2006). The ISL Langmuir probe experiment and its data processing onboard DEMETER: Scientific objectives, description and first results. *Planetary and Space Science*, *54*(5), 472–486. <https://doi.org/10.1016/j.pss.2005.10.017>
- Lee, C. C., Liou, Y. A., Otsuka, Y., Chu, F. D., Yeh, T. K., Hoshino, K., & Matunaga, K. (2008). Nighttime medium-scale traveling ionospheric disturbances detected by network GPS receivers in Taiwan. *Journal of Geophysical Research*, *113*(A12), A12316. <https://doi.org/10.1029/2008JA013250>
- Lee, W. K., Kil, H., & Paxton, L. J. (2021). Global distribution of nighttime MSTIDs and its association with E region irregularities seen by CHAMP satellite. *Journal of Geophysical Research: Space Physics*, *126*(5), e2020JA028836. <https://doi.org/10.1029/2020JA028836>
- Li, Q. B., Huang, Z., & Chen, S. (2020). A statistical analysis of global ionospheric E-layer scintillation during 2007–2014. *Radio Science*, *55*(8), 1–12. <https://doi.org/10.1029/2018RS006764>
- Makela, J. J., Vadas, S. L., Muryanto, R., Duly, T., & Crowley, G. (2010). Periodic spacing between consecutive equatorial plasma bubbles. *Geophysical Research Letters*, *37*(14), L14103. <https://doi.org/10.1029/2010GL043968>
- Martinis, C., Baumgardner, J., Mendillo, M., Wroten, J., MacDonald, T., Kosch, M., et al. (2019). First conjugate observations of medium-scale traveling ionospheric disturbances (MSTIDs) in the Europe-Africa longitude sector. *Journal of Geophysical Research: Space Physics*, *124*(3), 2213–2222. <https://doi.org/10.1029/2018JA026018>
- Martinis, C., Baumgardner, J., Wroten, J., & Mendillo, M. (2010). Seasonal dependence of MSTIDs obtained from the 630nm airglow imaging at Arecibo. *Geophysical Research Letters*, *37*(11), L11103. <https://doi.org/10.1029/2010GL043569>
- Moffat-Griffin, T., Hibbins, R. E., Jarvis, M. J., & Colwell, S. R. (2011). Seasonal variations of gravity wave activity in the lower stratosphere over an Antarctic Peninsula station. *Journal of Geophysical Research*, *116*(D14), D14111. <https://doi.org/10.1029/2010JD015349>
- Nanan, B., Chen, C. Y., Rajesh, P. K., Liu, J. Y., & Bailey, G. J. (2012). Modeling and observations of the low latitude ionosphere-plasmasphere system at long deep solar minimum. *Journal of Geophysical Research*, *117*(A8), A08316. <https://doi.org/10.1029/2012JA017846>
- Narayanan, V. L., Shiokawa, K., Otsuka, Y., & Neudegg, D. (2018). On the role of thermospheric winds and sporadic E layers in the formation and evolution of electrified MSTIDs in geomagnetic conjugate regions. *Journal of Geophysical Research: Space Physics*, *123*(8), 6957–6980. <https://doi.org/10.1029/2018JA025261>
- Nguyen, C. T. (2015). *Etude expérimentale de l'ionosphère de moyenne et basse latitude et de ses instabilités au moyen d'observations in-situ par DEMETER (Experimental study of the ionosphere at mid and low latitudes and of its instabilities by means of in situ observations from the DEMETER satellite)*. Thèse de Doctorat, University of Versailles Saint-Quentin.
- Ogawa, T., Ohtaka, K., Takami, T., Yamamoto, Y., Yamamoto, M., & Fukao, S. (1994). Medium and large scale TID's simultaneously observed by NNSS satellites and the MU radar. In F. S. Kuo (Ed.), *Low-Latitude Ionospheric Physics*, (Vol. 7, pp. 167–175). Elsevier Science.
- Otsuka, Y., Shinbori, A., Tsugawa, T., & Nishioka, M. (2021). Solar activity dependence of medium-scale travelling ionospheric disturbances using GPS receivers in Japan. *Earth Planets and Space*, *73*(1), 22–32. <https://doi.org/10.1186/s40623-020-01353-5>
- Otsuka, Y., Shiokawa, K., Ogawa, T., & Wilkinson, P. (2004). Geomagnetic conjugate observations of medium-scale traveling ionospheric disturbances at mid-latitude using all-sky airglow imagers. *Geophysical Research Letters*, *31*(15), L15803. <https://doi.org/10.1029/2004GL020262>



- Park, C. G. (1979). Comparison of two-dimensional and three-dimensional mapping of ionospheric electric field. *Journal of Geophysical Research*, *84*(A3), 960–964. <https://doi.org/10.1029/JA084iA03p00960>
- Park, J., Lühr, H., Kervalishvili, G., Rauberg, J., Michaelis, I., Stolle, C., & Kwak, Y.-S. (2015). Nighttime magnetic field fluctuations in the topside ionosphere at midlatitudes and their relation to medium-scale traveling ionospheric disturbances: The spatial structure and scale sizes. *Journal of Geophysical Research: Space Physics*, *120*(8), 6818–6830. <https://doi.org/10.1002/2015JA021315>
- Park, J., Lühr, H., Min, K. W., & Lee, J. J. (2010). Plasma density undulations in the nighttime mid-latitude F-region as observed by CHAMP, KOMPSAT-1, and DMSP F15. *Journal of Atmospheric and Solar-Terrestrial Physics*, *72*(2–3), 183–192. <https://doi.org/10.1016/j.jastp.2009.11.007>
- Park, J., Lühr, H., Stolle, C., Rodriguez-Zuluaga, J., Knudsen, D. J., Burchill, J. K., & Kwak, Y.-S. (2016). Statistical survey of nighttime midlatitude magnetic fluctuations: Their source location and Poynting flux as derived from the Swarm constellation. *Journal of Geophysical Research: Space Physics*, *121*, 11235–11248. <https://doi.org/10.1002/2016JA023408>
- Park, J., Lühr, H., Stolle, C., Rother, M., Min, K. W., Chung, J.-K., et al. (2009). Magnetic signatures of medium-scale traveling ionospheric disturbances as observed by CHAMP. *Journal of Geophysical Research*, *114*(A3), A03307. <https://doi.org/10.1029/2008JA013792>
- Parrot, M. (2006). First results of the DEMETER micro-satellite. *Planetary and Space Science*, *54*, 5–412. <https://doi.org/10.1016/j.pss.2005.10.012>
- Paulino, I., Medeiros, A. F., Vadas, S. L., Wrasse, C. M., Takahashi, H., Burity, R. A., et al. (2016). Periodic waves in the lower thermosphere observed by OI 630nm airglow images. *Annales Geophysicae*, *34*(2), 293–301. <https://doi.org/10.5194/angeo-34-293-2016>
- Perkins, F. (1973). Spread F and ionospheric currents. *Journal of Geophysical Research*, *78*(1), 218–226. <https://doi.org/10.1029/JA078i001p00218>
- Saito, A., Fukao, S., & Miyazaki, S. (1998). High resolution mapping of TEC perturbations with GSI GPS network over Japan. *Geophysical Research Letters*, *25*(16), 3079–3082. <https://doi.org/10.1029/98GL52361>
- Saito, A., Iyemori, T., Blomberg, L. G., Yamamoto, M., & Takeda, M. (1998). Conjugate observations of the mid-latitude electric field fluctuations with the MU radar and the Freja satellite. *Journal of Atmospheric and Solar-Terrestrial Physics*, *60*(1), 129–140. [https://doi.org/10.1016/s1364-6826\(97\)00094-1](https://doi.org/10.1016/s1364-6826(97)00094-1)
- Saito, A., Iyemori, T., Sugiura, M., Maynard, N. C., Aggson, T. L., Brace, L. H., et al. (1995). Conjugate occurrence of the electric field fluctuations in the nighttime mid-latitude ionosphere. *Journal of Geophysical Research*, *100*(A11), 21439–21451. <https://doi.org/10.1029/95ja01505>
- Saito, A., Nishimura, M., Yamamoto, M., Fukao, S., Kubota, M., Shiokawa, K., et al. (2001). Traveling ionospheric disturbances detected in the FRONT campaign. *Geophysical Research Letters*, *28*(4), 689–692. <https://doi.org/10.1029/2000gl011884>
- Shibata, T., & Okuzawa, T. (1983). Horizontal velocity dispersion of medium-scale travelling ionospheric disturbances in the F-region. *Journal of Atmospheric and Terrestrial Physics*, *45*(2–3), 149–159. [https://doi.org/10.1016/s0021-9169\(83\)80019-1](https://doi.org/10.1016/s0021-9169(83)80019-1)
- Shimeis, A., Fathy, I., Amory-Mazaudier, C., Fleury, R., Mahrous, A. M., Yumoto, K., & Groves, K. (2012). Signature of the coronal hole on near the North crest equatorial anomaly over Egypt during the strong geomagnetic storm 5th April 2010. *Journal of Geophysical Research*, *117*(A7), A07309. <https://doi.org/10.1029/2012JA017753>
- Shiokawa, K., Ihara, C., Otsuka, Y., & Ogawa, T. (2003). Statistical study of nighttime medium-scale traveling ionospheric disturbances using mid-latitude airglow images. *Journal of Geophysical Research*, *108*(A1), 1052. <https://doi.org/10.1029/2002JA009491>
- Shiokawa, K., Ihara, C., Otsuka, Y., Ogawa, T., & Rich, F. J. (2003). Ground and satellite observations of nighttime medium-scale traveling ionospheric disturbances using mid-latitude airglow images. *Journal of Geophysical Research*, *108*(A1), 1145. <https://doi.org/10.1029/2002JA009639>
- Shiokawa, K., Otsuka, Y., Ejiri, M. K., Sahai, Y., Kadota, T., Ihara, C., et al. (2002). Imaging observations of the equatorward limit of MSTID. *Earth Planets and Space*, *54*(1), 57–62. <https://doi.org/10.1186/bf03352421>
- Shiokawa, K., Otsuka, Y., Sugawa, T., Ogawa, T., Saito, A., Ohshima, K., et al. (2005). Geomagnetic conjugate observation of nighttime medium-scale and large-scale traveling ionospheric disturbances: FRONT3 campaign. *Journal of Geophysical Research*, *110*(A5), A05303. <https://doi.org/10.1029/2004JA010845>
- Sivakandan, M., Chakrabarty, D., Ramkumar, T. K., Guharay, A., Taori, A., & Perihar, N. (2019). Evidence for deep ingressions of the midlatitude MSTID into as low as 3.5° magnetic latitude. *Journal of Geophysical Research: Space Physics*, *124*(1), 749–764. <https://doi.org/10.1029/2018JA026103>
- Solomon, S. C., Qian, L., & Burns, A. G. (2013). The anomalous ionosphere between solar cycles 23 and 24. *Journal of Geophysical Research: Space Physics*, *118*(10), 6524–6535. <https://doi.org/10.1002/jgra.50561>
- Tsuchiya, S., Shiokawa, K., Otsuka, Y., Nakamura, T., Yamamoto, M., Connors, M., et al. (2020). Wavenumber spectra of atmospheric gravity waves and medium-scale traveling ionospheric disturbances based on more than 10-year airglow images in Japan, Russia, and Canada. *Journal of Geophysical Research: Space Physics*, *125*(3), e2019JA026807. <https://doi.org/10.1029/2019JA026807>
- Tsugawa, T., Otsuka, Y., Coster, A. J., & Saito, A. (2007). Medium-scale traveling ionospheric disturbances detected with dense and wide TEC maps over USA. *Geophysical Research Letters*, *34*(22), L22101. <https://doi.org/10.1029/2007GL031663>
- Tsunoda, R. T. (2006). On the coupling of layer instabilities in the nighttime mid-latitude ionosphere. *Journal of Geophysical Research*, *111*(A11), A11304. <https://doi.org/10.1029/2006JA011630>
- Tsunoda, R. T., & Cosgrove, R. B. (2001). Coupled electrodynamics in the nighttime midlatitude ionosphere. *Geophysical Research Letters*, *28*(22), 4171–4174. <https://doi.org/10.1029/2001gl013245>
- Tsunoda, R. T., Cosgrove, R. B., & Ogawa, T. (2004). Azimuth-dependent Es layer instability: A missing link found. *Journal of Geophysical Research*, *109*(A12), A12303. <https://doi.org/10.1029/2004JA010597>
- Vadas, S. L., & Becker, E. (2018). Numerical modeling of the excitation, propagation, and dissipation of primary and secondary gravity waves during wintertime at McMurdo Station in the Antarctic. *Journal of Geophysical Research: Atmospheres*, *123*(17), 9326–9369. <https://doi.org/10.1029/2017JD027974>
- Vadas, S. L., & Becker, E. (2019). Numerical modeling of the generation of tertiary gravity waves in the mesosphere and thermosphere during strong mountain wave events over the southern Andes. *Journal of Geophysical Research: Space Physics*, *124*(9), 7687–7718. <https://doi.org/10.1029/2019JA026694>
- Vadas, S. L., Zhao, J., Chu, X., & Becker, E. (2018). The excitation of secondary gravity waves from local body forces: Theory and observation. *Journal of Geophysical Research: Atmospheres*, *123*(17), 9296–9325. <https://doi.org/10.1029/2017JD027970>
- Valladares, C. E., & Hei, M. A. (2012). Measurement of the characteristics of TIDs using small and regional networks of GPS receivers during the campaign of 17–30 July of 2008. *International Journal of Geophysics*, *2012*, Article ID 548784. <https://doi.org/10.1155/2012/548784>
- Wickert, J., Pavelyev, A. G., Liou, Y., Schmidt, T., Reigber, C., Igarashi, K., et al. (2004). Amplitude variations in GPS signals as a possible indicator of ionospheric structures. *Geophysical Research Letters*, *31*(24), L24801. <https://doi.org/10.1029/2004GL020607>
- Wu, D. L., Ao, C. O., Hajj, G. A., de la Torre Juarez, M., & Manucci, A. J. (2005). Sporadic E morphology from GPS-CHAMP radio occultation. *Journal of Geophysical Research*, *110*(A1), A01306. <https://doi.org/10.1029/2004JA010701>

- Yokoyama, T. (2013). Scale dependence and frontal formation of nighttime medium-scale traveling ionospheric disturbances. *Geophysical Research Letters*, *40*(17), 4515–4519. <https://doi.org/10.1002/grl.50905>
- Yokoyama, T. (2014). Hemisphere-coupled modeling of nighttime medium-scale traveling ionospheric disturbances. *Advances in Space Research*, *54*(3), 481–488. <https://doi.org/10.1016/j.asr.2013.07.048>
- Yokoyama, T., & Hysell, D. L. (2010). A new mid-latitude ionosphere electrodynamic coupling model (MIECO): Latitudinal dependence and propagation of medium-scale traveling ionospheric disturbances. *Geophysical Research Letters*, *37*(8), L08105. <https://doi.org/10.1029/2010GL042598>
- Yokoyama, T., Hysell, D. L., Otsuka, Y., & Yamamoto, M. (2009). Three-dimensional simulation of the coupled Perkins and Es layer instabilities in the nighttime mid-latitude ionosphere. *Journal of Geophysical Research*, *114*(A3), A03308. <https://doi.org/10.1029/2008JA013789>
- Yu, B., Xue, X., Yue, X., Yang, C., Yu, C., Dou, X., et al. (2019). The global climatology of the intensity of the ionospheric sporadic E layer. *Atmospheric Chemistry and Physics*, *19*(6), 4139–4151. <https://doi.org/10.5194/acp-19-4139-2019>
- Zerbo, J.-L., Amory-Mazaudier, C., & Ouattara, F. (2012). Geomagnetism during solar cycle 23: Characteristics. *Journal of Advanced Research*, *4*(3), 256–274. <https://doi.org/10.1016/j.jare.2012.08.010>